U.S. Geological Survey Award No.
G19AP00058

Final Technical Report

IMPROVING THE ASSESSMENT OF SITE-SPECIFIC SEISMIC HAZARDS THROUGH THE LENS OF NOVEL ATTENUATION MODELS

Principal Investigator:
Ashly Cabas[1]
Graduate Research Assistant:
Chunyang Ji[2]

Project Start/End Dates: 15 May 2019/14 April 2020

[1] Assistant Professor
North Carolina State University
Civil, Construction, and Environmental Engineering
425A Mann Hall, 2501 Stinson Drive
Raleigh, NC 27695-7908
Tel: (919) 515-7338
Email: amcabasm@ncsu.edu

[2] Ph.D. Student
North Carolina State University
Civil, Construction, and Environmental Engineering
208 Mann Hall, 2501 Stinson Drive
Raleigh, NC 27695-7908
Email: cji3@ncsu.edu

Acknowledgment of support and disclaimer: This material is based upon work supported by the U.S. Geological Survey under Grant No. G19AP00058. The views and conclusions contained in this document are those of the authors and should not be interpreted as representing the opinions or policies of the U.S. Geological Survey. Mention of trade names or commercial products does not constitute their endorsement by the U.S. Geological Survey.

Abstract

Site-specific attenuation can be defined by means of the distance-independent spectral decay parameter κ_0 (Anderson and Hough, 1984). However, estimates of κ_0 are currently burdened with uncertainties including the ones associated with calculations at a single site, estimates beyond the linear-elastic elastic regime, and model-to-model variability. This report describes the work done under grant number G19AP00058, entitled "Improving the Assessment of Site-specific Seismic Hazards Through the Lens of Novel Attenuation Models" and it is presented in three parts.

Part I investigates the variability in kappa, κ, estimates at a single station (what we refer to as within-station variability). A better understanding of potential factors that lead to large scatter in estimated values of κ constitutes a critical need for ground motion modeling and seismic hazard assessment at large. Most research efforts to date have focused on studying the site-to-site variability of κ, but the uncertainties in individual κ estimations associated with different events at a selected site remain uncharacterized. This part is reproduced from an article written by the same authors (in collaboration with Drs. Fabrice Cotton, Marco Pilz, and Dino Bindi from the German Center of Geosciences at Potsdam, Germany) and published in the Bulletin of the Seismological Society of America (BSSA) in April 2020 (https://doi.org/10.1785/0120190253).

Part II aims to quantify near-surface attenuation (as captured by κ) beyond the linear-elastic regime. Soil nonlinear behavior, often triggered in soft sedimentary deposits subjected to strong ground shaking has led to catastrophic damage to civil infrastructure in many past earthquakes. Nonlinear behavior in soils is associated with larger shear strains, increased material damping ratio and reduced stiffness. However, most investigations of the high-frequency spectral decay parameter κ, have focused on low-intensity ground motions inducing only small shear strains. Because studies of the applicability of κ when larger deformations are induced are rather limited, we investigate the behavior of κ (both, individual κ_r and site-specific κ_0 estimates) beyond the linear-elastic regime. This second part of the completed work was submitted to the BSSA special section on Advances in Site Response and it was still under review by the time of publication of this final technical report. Dr. Luis Fabian Bonilla and Dr. Celine Gelis from IFSTTAR and IRSN, respectively, are co-authors of this portion of the study.

Part III explores model-to-model variability in κ values and provides recommendations for future research addressing limitations and challenges identified for the different approaches considered. Particularly, this study focuses on the challenges associated with the lack of data in low-to-moderate seismicity regions, which does not allow the use of the classical acceleration spectrum methodology to compute individual values of κ in the Fourier Amplitude Spectrum of multiple ground motion recordings. This part of the study was conducted in collaboration with Dr. Linda Al Atik, Dr. Abhinav Gupta and PhD student Sugandha Singh from NCSU.

Table of Contents

Part I: Within-Station Variability in Kappa: Evidence of Directionality Effects

1. Introduction

The characterization of attenuation at various scales (from regional to local) constitutes a critical component in the prediction of ground motions, site response analysis and seismic hazard assessments. Thus, understanding ground motion characteristics at high frequencies has become a research focus in recent studies (e.g., Mayor et al. 2018; Parolai 2018). The high-frequency decay parameter, κ, was proposed by Anderson and Hough (1984) to characterize linear decay of the shear-waves (S-wave) Fourier acceleration amplitude spectrum (FAS) in log-linear scale in the high-frequency range. In general, individual estimations of κ values, hereafter referred to as κ_r, are decomposed into a site-specific component, κ_0, a generalized distance-dependency component, κ_R, and a source component, κ_s (Ktenidou et al. 2014).

The site-specific component, κ_0, captures the attenuation taking place directly below the site of interest (Ktenidou et al. 2013), but further investigation is required to define the depth of the geologic profile that contributes toward the κ_0 resulting at the ground surface. Ground motion models and their adjustments from host to target regions have used estimates of κ_0 to characterize the effects of high frequency attenuation (e.g., Van Houtte et al. 2011, Campbell 2003, Ktenidou et al. 2014). Moreover, knowledge of κ_0 benefits the identification of epistemic uncertainties to remove the ergodic assumption in site-specific probabilistic seismic hazard analysis (PSHA), which is crucial for the seismic design of critical facilities such as nuclear power plants (Rodriguez-Marek et al. 2014, Cabas and Rodriguez-Marek 2017). Deciphering the physics behind empirical estimates of κ_0 requires understanding the site's contribution to the overall attenuation. Decoupling local and regional attenuation mechanisms will facilitate the development of physics-based ground motion simulations and non-ergodic ground motion prediction equations (GMPEs).

Previous studies have investigated the correlation between κ_0 and other site parameters, such as the time-averaged shear-wave velocity of the top 30 m subsoil (V_{s30}) (e.g., Van Houtte et al. 2011, 2014, Ktenidou et al. 2015, Cabas et al. 2017), but large uncertainties in κ_r estimations (which also affect the computation of κ_0) impose difficulties to unveil the physical meaning of κ_0 (Perron et al. 2017). An understanding of the sources of variability affecting κ_r and κ_0 constitutes a crucial step toward robust and sustainable applications of κ_0 in earthquake engineering practice.

The variability of κ has been studied through different lenses in the last decade, from model-to-model variability (e.g., Ktenidou et al. 2014, Edwards et al. 2015, Perron et al. 2017), user-to-user variability (e.g., Edwards et al. 2015, Douglas et al. 2010), to site-to-site variability (e.g., Van Houtte et al. 2011, 2014, Cabas et al. 2017). Some have investigated the variability in κ_r and κ_0 estimates when utilizing a single methodology, but incorporating alternative assumptions throughout the implementation (e.g., Ktenidou et al. 2013). Other efforts have focused on understanding the correlation (or lack thereof) among different methods to obtain κ_0 (e.g.,

Ktenidou et al. 2014, Perron et al. 2017). Whilst, the variability of κ_0 as a function of site conditions have been extensively studied for multiple regions, including Japan, Greece, France and the US (e.g., Douglas et al. 2010, Laurendeau et al. 2013, Ktenidou et al. 2015, Cabas et al. 2017, Parolai 2018).

The objective of this study is to characterize the within-station variability of κ_0. Ten stations from the Japanese database, KiK-net, are investigated. Their corresponding National Earthquake Hazards Reduction Program (NEHRP) site class classification varies from B (rock) to D (stiff soils). First, we introduce a framework to evaluate aleatory variability and epistemic uncertainty in κ_r and κ_0. Then, we focus on individual values of κ_r calculated following the traditional approach by Anderson and Hough (1984) at the ten study sites, and investigate how ground motion directionality affects the estimation of κ_r. Finally, we explore the influence of earthquake type and focal depth on the estimates of κ_R and κ_0. Within one selected station, we find that values of κ_R and κ_0 are affected by repeatable contributions from the path, with these path effects being more significant for κ_R.

2. Uncertainty and Variability in Kappa

Empirical data from multiple seismic events and recording stations are used to construct ground motion models (GMM) that can describe the distribution of ground motion in terms of a median and a logarithmic standard deviation, σ (Al Atik et al. 2010). The aleatory variability in the ground motion, represented by σ has proven to exert a strong influence on hazard estimates, especially at low annual exceedance frequencies (Bommer and Abrahamson 2006, Al Atik et al., 2010, Rodriguez-Marek et al., 2014). Defensible reductions in σ are desirable not only because of their ultimate effect on PSHA, but also because they result from a clear separation of aleatory variability (which is theoretically irreducible) and epistemic uncertainty (which can be reduced with the collection of new data, Rodriguez-Marek et al. 2014). In pursuit of defensible reductions in σ, repeatable source, path, and/or site contributions can be identified at a single site and invoke the nonergodic assumption. The ergodic assumption implies that the temporal distribution of ground motions at a given site is equivalent to the spatial distribution of ground motions across many sites (given the same causal parameters, Kuehn et al. 2019).

In this study, we focus on identifying repeatable site and path contributions to the observed variability in κ_r, κ_R and κ_0. Drawing parallels to the residual analysis process in ground motion modeling, this work aims to provide a characterization of the within-station variability in κ_r and κ_0 estimates, which can further support the development of the site-term parameterization in nonergodic GMMs. Baltay et al. (2017) provided evidence of a correlation between κ_0 values and the average site residual, using small-magnitude ground motion data recorded at ten stations from the ANZA network. Estimates of κ_0 could inform predictions of station-specific site residuals in partially nonergodic GMMs "to improve our physical understanding of the site term at specific stations" (Baltay et al. 2017). We select a subset of recordings at selected stations from the KiK-net database to identify and quantify systematic, repeatable contributions to κ_r, κ_R and κ_0 estimates; hereafter referred to as within-station variability in κ.

Approaches to estimate κ_0 can be classified into two types, namely direct estimates and empirical estimates from statistical regressions. Factors that introduce variability in κ_0 estimates for each type are grouped into six categories with considerations of model selections, database choices and record processing protocols as shown in **Figure 1**. The latter provides a framework to investigate epistemic uncertainties in κ_0 estimates for the linear elastic regime only. Further research is required should soil nonlinearity be triggered. The description of each category depicted in **Figure 1** is presented below.

- Part 1 κ_0-model

  The commonly used statistical regression approach is based on a linear distance-dependent model, where κ_0 represents the site-specific component, while κ_R refers to the regional attenuation. Values of κ_0 and κ_R are obtained via empirical linear regression of κ_r following the Anderson and Hough (1984) method. Alternatively, direct estimates of κ_0 can be obtained from the site properties (e.g., measurements of κ_0 in the high frequency decay of a transfer function, Drouet et al. 2010) without the definition of the κ_0- linear regression model. The choice of a linear regression as opposed to other possible functional forms has been mostly based on the simplicity of the model and observed fit to the empirical data (Ktenidou et al 2013).

- Part 2 depth-dependency

  The measured κ_0 values can be depth-dependent or thickness–dependent based on the approach selected for the respective calculations. Values of κ_0 provide an estimate of attenuation directly below the depth at which the ground motions are recorded. Different κ_0 values are typically obtained at different depths within a site profile (e.g., Ktenidou et al 2015). Values of site-specific κ_0 have also been proposed to represent the contribution of a specific soil column with a given thickness (e.g., Campbell 2009).

- Part 3 approach choice

  Previous studies show that various kappa calculation approaches will result in different individual κ_r values (for the same ground motion), and ultimately different κ_0 estimates (e.g., Ktenidou et al 2014). Understanding the suitability of each method in consideration of the available records and site conditions is relevant to reduce uncertainties in kappa estimations. In Figure 1, κ_{r_BB}, κ_{r_DS} and κ_{r_AS} refer to individual values of kappa from the broadband method (Ktenidou et al., 2016), the displacement method (Biasi and Smith, 2001), and the acceleration spectrum method (Anderson and Hough 1984), respectively. Direct measurement approaches also shown in Figure 1 include estimations of κ_0 from the response spectrum, κ_{0_RESP} (Silva and Darragh 1995), utilizing inverse random vibration theory, κ_{0_IRVT} (Al Atik et al 2014), and from the site's transfer function, κ_{0_TF} (Drouet et al 2010).

- Part 4 dataset choice

Choosing an appropriate dataset can reduce the within-station variability in κ_0 by constraining the uncertainties associated with individual κ_r values. In general, only magnitude, source-to-site distance, and type of seismicity are used to select appropriate ground motions for kappa calculations. However, we hypothesize that considering the events' azimuth, and focal depths can provide insights on other sources of within-station variability.

- Part 5 record processing

  The variability associated with record processing refers to differences stemming from the usage of the S-wave window or the whole time series to calculate κ_r values. Anderson and Hough (1984) originally introduced the calculation of κ_{r_AS} as the linear decay of the S-wave FAS in the high frequency range. However, varying selections of the S-wave window can introduce additional scatter in κ_r for the same event (Douglas et al. 2010, Cabas et al. 2017, Xu et al. 2019). This additional variability may be caused by the assumed duration of the selected S-wave window or by the explicit consideration of the direct S-wave only or the direct S-wave window and coda/surface waves. Values of κ_{r_AS} estimated from the S-wave window could be significantly biased by scattering effects, except when intrinsic attenuation is dominant (Parolai et al. 2015, Pilz and Fah 2017, Parolai 2018, Pilz et al. 2019).

- Part 6 spectrum processing

  The estimation of κ_{r_AS} is significantly sensitive to the selection of frequency ranges, including: (1) the length of the frequency band; (2) local site conditions such as site-amplification peaks (Parolai and Bindi 2004); and (3) the presence of multiple linear decay trends in the high frequency range of the FAS. Using smoothen FAS instead of the original FAS also introduces differences for κ_r estimates. Additionally, there is variability resulting from different approaches to treat recorded horizontal components. For instance, (a) treating orthogonal horizontal components independently (Dimitriu et al. 2001), (b) averaging κ_{r_AS} values estimated from as-recorded horizontal components if differences in these κ_{r_AS} values are less than 20% (Ktenidou et al. 2013), and (c) averaging κ_{r_AS} values estimated from as-recorded horizontal components without consideration of the corresponding differences in individual κ_{r_AS}.

We would like to emphasize that the ultimate influence of the aforementioned sources of variability is usually station-dependent, although the logic tree and framework described in **Figure 1** can be implemented at any site. Thus, the significance of each branch is unique for a given site, which results in a better characterization of the within-station variability at the site. In this paper, we only focus on the branches highlighted in **Figure 1**. The Anderson and Hough (1984) method is used to investigate systematic contributions to the variability in κ_r (hereafter referred to as κ_{r_AS}) and κ_0. We investigate the within-station variability caused by (1) the dataset choice (part 4) based on earthquake types and focal depths, and (2) spectrum processing (part 6) by understanding the contributions of ground motion directionality.

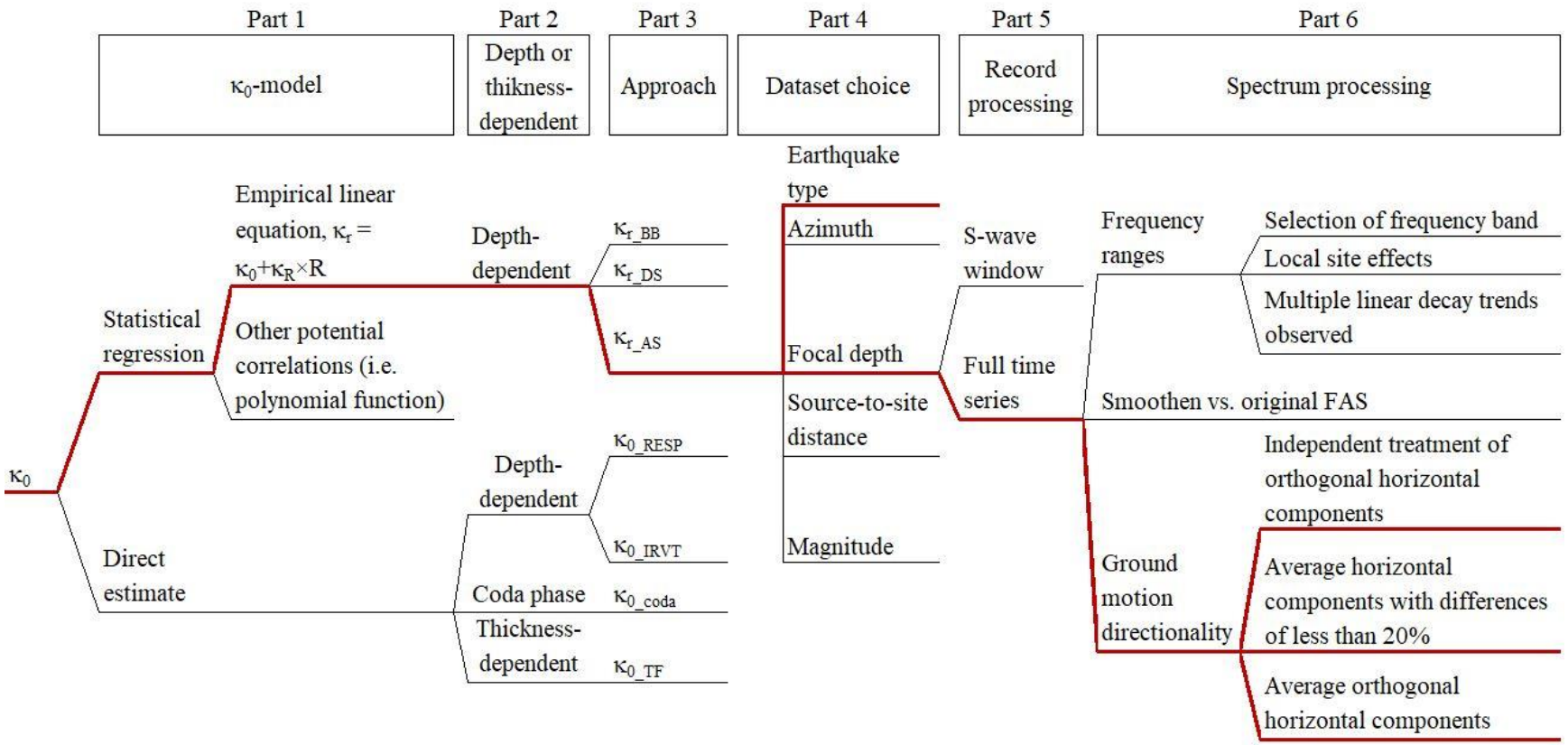

Figure 1. Logic tree for the estimation of κ_0 values. The highlighted branches are explored in this work.

3. Database Description and Study sites

We use the Japanese Kiban-Kyoshin network (KiK-net) database (see Data and Resources Section), which is a strong-motion seismograph network uniformly deployed at more than 600 locations in Japan and able to provide high-quality data at various site classes. KiK-net has a pair of seismographs at each station, one located on the ground surface, and the other one in a borehole together with high-sensitivity (Hi-net) seismographs. The depth of each borehole sensor is typically between 100 m and 200 m. Instrumental sampling frequencies are 100 Hz or 200 Hz. Wave velocity profiles (for both P-wave and S-wave) at each station are measured by downhole PS logging, and the corresponding files are available on the KiK-net website (see Data and Resources). The orientations of orthogonal ground surface sensors are north-south and east-west. However, difficulties during installation and regular maintenance at some stations may have changed the orientations of borehole sensors (Aoi et al. 2004, Aoi et al. 2011). The azimuths of borehole sensors at each KiK-net station are available on the Hi-net website (see Data and Resources). The entire dataset and flatfile used in this paper is built and compiled with an automated protocol by Dawood et al. (2016). The seismic moment magnitude M_w, focal depth, epicenter location and focal mechanism information are obtained from the NIED moment tensor solution available at the broadband seismography network (F-net) catalogue.

In this paper, recorded horizontal components at the ground surface and at depth are used. The criteria for selection of ground motions and stations include: (1) epicentral distances less than 150 km; (2) M_w larger than 4.0; (3) peak ground acceleration (PGA) values at the surface less than 0.01 g (to avoid effects of soil nonlinearity); (4) at least 50 available records complying with requirements (1) to (3) per study site; (5) the signal-to-noise ratio (SNR) larger 3.0 over the frequency ranges for κ_{r_AS} estimation. Moreover, the ability of shear-wave velocity profiles measured by downhole logging at KiK-net stations to describe actual site conditions has been questioned in the past (Wu et al. 2017). 2D/3D wave propagation could be significant at some KiK-Net stations because of the edge-generated surface waves, topographic effects and focusing effects. However, the potential for site scattering effects can be reduced as we considered KiK-Net sites with reliable shear wave velocity (V_s) profiles that meet the 1D wave propagation assumptions based on the results from Pilz and Cotton (2019). Thus, ten stations corresponding to various site classes (NEHRP site class from B to D) are selected in this study. Key characteristics pertaining these study sites are provided in **Figure 2** and **Table 1**.

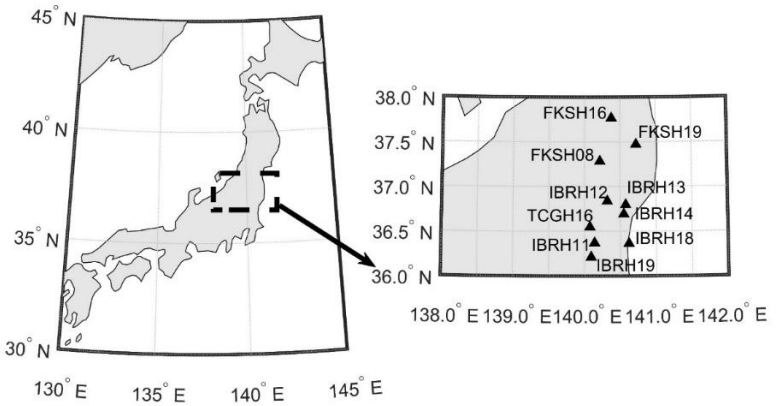

Figure 2. Locations of each selected Japanese station in this study.

Table 1. Selected stations information.

Station Name	Station Latitude	Station Longitude	*V_{s30}	†Hole Depth	††H_{800}	Borehole Sensor Azimuth	§NEHRP Site Class
	degree	degree	m/s	m	m	degree	
FKSH08	37.28	140.22	562.50	105	8	-3	C
FKSH16	37.76	140.38	531.61	300	180	1	C
FKSH19	37.47	140.73	338.06	100	20	-4	D
IBRH11	36.37	140.14	242.49	103	30	0	D
IBRH12	36.83	140.32	485.71	200	20	-3	C
IBRH13	36.79	140.58	335.37	100	34	2	D
IBRH14	36.69	140.55	829.12	100	10	-1	B
IBRH18	36.36	140.62	558.56	504	30	0	C
IBRH19	36.21	140.09	692.31	210	2	-1	C
TCGH16	36.54	140.08	213.20	112	NaN	-2	D

*V_{s30}: the time-averaged shear-wave velocity of the top 30 m subsoil
†Hole-depth: the depth of borehole sensor relative to the ground surface
††H_{800}: depth to a horizon with velocity V_s of 800 m/s or more
§NEHRP Site Class: National Earthquake Hazards Reduction Program (NEHRP) site class classification

4. Methods

4.1. Estimation of κ_r and κ_0

We use the acceleration spectrum approach (Anderson and Hough, 1984) to estimate κ_{r_AS}. The slope of the linear decay, $-\pi\kappa_{r\_AS}$, of the acceleration FAS in the high frequency range using log-linear coordinates is calculated for each horizontal component of the selected records. A weighted robust least square linear regression with Bisquare function over a manually selected high-frequency range ($[f_1, f_2]$) (see **Figure 3** as an example). The minimum difference between f_1 and f_2 is 8 Hz. Following the recommendations of Ktenidou et al. (2013), f_1 is larger than the corresponding earthquake source-corner frequency (f_c), computed by Equation (1) (Brune, 1970, 1971):

$$f_c = 4.9\times10^4 \beta \left(\frac{\Delta\sigma}{M_0}\right)^{\frac{1}{3}} \quad (1)$$

Where f_c is in Hz, β is the shear-wave velocity near the source with units of km/s, $\Delta\sigma$ is the stress drop in MPa, and M_0 is the seismic moment in N·m. In this article, β is assumed to be 3.6 km/s (Pei et al. 2009). The value of $\Delta\sigma$ is assumed to be 3 MPa for crustal earthquakes and 5.5 MPa for subduction zone events (Nakano et al. 2015). Moreover, because the instrument's response is approximately flat below 30 Hz (which is close to the response of a three-pole Butterworth filter with a cutoff frequency of 30 Hz), we restrict f_2 to be less than 30 Hz (Aoi et al. 2004, Fujiwara et al. 2004, Oth et al. 2011, Laurendeau et al, 2013,Cabas et al. 2017).

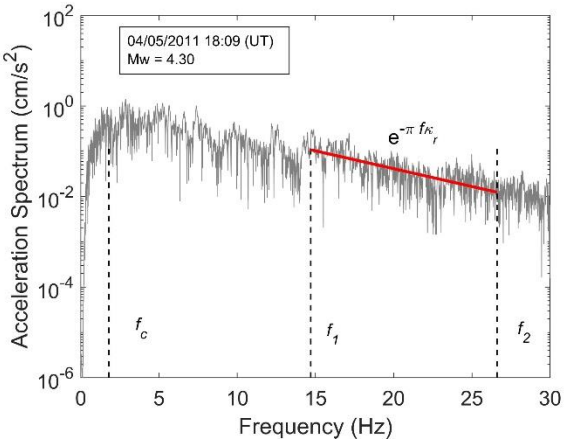

Figure 3. Selection of f_1 and f_2 on the Fourier acceleration amplitude spectrum corresponding to a surface record at station IBRH20. f_c refers to the corner frequency as estimated by the Brune (1970) model with stress drop of 3.0 MPa for active crustal events.

The S-wave window is often used to estimate κ_{r_AS}. Previous studies have picked the direct S-wave manually assuming a minimum duration of 5 sec for small/nearby events and 20 sec for large/far events (Ktenidou et al. 2013). Whilst, others have included the coda wave within the selected S-wave window for records where the coda wave cannot be separated clearly (Anderson and Hough 1984). Differences in κ_{r_AS} (computed by the acceleration spectrum approach using the whole time series) and $\kappa_{r\_AS\_SW}$ (computed by the acceleration spectrum approach using manually selected S-wave windows, following Anderson and Hough (1984)) are compared for records from shallow crustal earthquakes used in this study (see **Figure 4**). The same frequency range, f_1 and f_2, is applied to each record to avoid bias from frequency range selections. The ratio, $r_1 = \kappa_{r\_AS}/\kappa_{r\_AS\_SW}$, is computed at each study site to represent the differences between κ_{r_AS} and $\kappa_{r\_AS\_SW}$ in **Figure 4**. Values of $\kappa_{r\_AS\_SW}$ are generally larger than κ_{r_AS} at the study sites (i.e., r_1 is generally less than 1.0). Scattering effects can help explain observed lower κ_{r_AS} values from the whole time series. When intrinsic attenuation is strong at a given site, higher frequencies can be removed more efficiently resulting in a steep slope in the S-wave FAS (Parolai et al. 2015). The full time series is composed of the direct S-waves, but also scattered waves from the redistribution of the seismic waves' energy. The latter can modify the slope in the FAS at high frequencies producing a biasedκ_{r_AS}, which generally is lower. Moreover, the S-wave window dominates the spectrum at surface and the downgoing waves could more affect the borehole time series. Thus, more variations between κ_{r_AS} and $\kappa_{r\_AS\_SW}$ at depth are observed. Because the differences between $\kappa_{r\_AS\_SW}$ and κ_{r_AS} are less than 20% for most of the selected ground motions used in this study, we choose the full time series to estimate κ_{r_AS} values. Further guidance in the selection of the S-wave window for kappa calculations can provide meaningful insights to reduce the between-station variability in kappa.

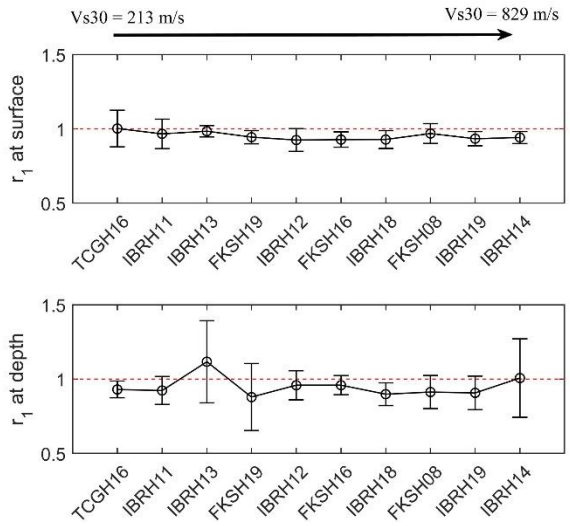

Figure 4. Comparison between κ_{r_AS} (from the whole FAS) and $\kappa_{r\_AS\_SW}$ (from the S-wave window FAS) corresponding to our ten study sites. r_1 is the ratio computed by $\kappa_{r\_AS}/\kappa_{r\_AS\_SW}$. The dash line represents a ratio of 1.0. The circles depict the mean r_1 of all observed records, and the error bars indicate the +/- standard derivation of all observed ratios at each site of interest.

We choose the linear κ_0-model introduced by Anderson (1991) and follow the nomenclature proposed by Ktenidou et al. (2013) to estimate the site component κ_0:

$$\kappa_{r\_AS} = \kappa_0 + \kappa_R \cdot R_{epic} \tag{2}$$

Where the κ_{r_AS}, and κ_0 are expressed in units of time (s), κ_R in units of s/km, and R_{epic} is the epicentral distance in km. This κ_0-model assumes a unique source-to-site path for each record, and a homogeneous, frequency-independent seismic quality factor, Q (Knopoff 1964). Thus, we only select events with epicentral distances less than 150 km to minimize the potential for multiple source-to-site ray paths per record. The assumption of a unique Q-value allows for the calculation of κ_R (following the linear model in Equation (2)), which describes regional attenuation. Japan has varying Q-values across the region, with lower Q-values in the central Japanese island and higher Q-values on the east coast (Pei et al. 2009, Nakano et al. 2015). The low Q- and high Q-value regions are separated by Japan's volcanic belt. Thus, we avoid using records that cross the volcanic belt during their propagation path from source to site based on the attenuation classification map provided by Nakano et al. (2015). The κ_0-model in Equation (2) is also based on the assumption that the source contribution is negligible (Ktenidou et al. 2014, Van Houtte et al. 2011). For the selected KiK-net stations, the path component, κ_R, is constrained to be the same for both surface and borehole records because the regional attenuation contributions should be identical when analyzing individual stations (Ktenidou et al. 2013, 2015, Cabas et al. 2017). We use the maximum likelihood method to model κ_{r_AS} with the constrained κ_R based on Equation (2).

4.2. Ground Motion Directionality

A recorded ground motion at a specific site can vary depending on sensor orientation (Boore et al. 2006). This lack of uniformity of ground motions in all possible orientations is known as ground

motion directionality. Two as-recorded horizontal orthogonal components of each selected ground motion are rotated to study the influence of ground motion directionality on the estimation of κ_{r_AS}. All records are rotated using the following equations (Boore et al. 2006, Boore 2010):

$$a_{ROT\_1}(t;\theta) = a_1(t)\cos(\theta) + a_2(t)\sin(\theta) \tag{3}$$

$$a_{ROT\_2}(t;\theta) = -a_1(t)\sin(\theta) + a_2(t)\cos(\theta) \tag{4}$$

Where $a_1(t)$ and $a_2(t)$ are the as-recorded acceleration time series, $a_{ROT\_1}(t;\theta)$ and $a_{ROT\_2}(t;\theta)$ are the rotated motions with the corresponding rotation angle θ. The κ_{r_AS} values computed from the corresponding FAS of rotated motions are referred to as $\kappa_{r\_AS\_ROT}$. In this article, we only rotate one single horizontal component ($a_1(t)$ or $a_2(t)$) from 0° to 180° (i.e., non-redundant angles) with increments of 10° to investigate the influence of ground motion directionality on κ_{r_AS}.

Considering that the frequency range ([f_1, f_2]) to estimate κ_{r_AS} is selected visually for each event, a large number of calculations is required for $\kappa_{r\_AS\_ROT}$ estimations. Thus, we propose a semi-automatic algorithm to compute $\kappa_{r\_AS\_ROT}$. First, we select the frequency range based on visual inspection of the as-recorded motion from a given event (at a given site). Then, a common frequency range is selected for the pair of recorded horizontal components and applied to all the corresponding rotated motions from that same event at that station. The main advantage of the proposed procedure, beyond the optimization of the computational process, is that it avoids the introduction of additional uncertainties stemming from the frequency range selection. The performance of the proposed semi-automatic algorithm is evaluated by visually inspecting the rotated FAS plots and the corresponding frequency range.

The influence of ground motion directionality on the attenuation contributed by the soil column, hereafter referred to as $\Delta\kappa(\theta)$, is also investigated. $\Delta\kappa(\theta)$ is calculated as follows, assuming the κ_R value remains unchanged:

$$\begin{aligned}\Delta\kappa(\theta) &= \kappa_{r\_AS\_ROT\_sur}(\theta) - \kappa_{r\_AS\_ROT\_bore}(\theta) \\ &= (\kappa_{0\_ROT\_sur}(\theta) + \kappa_R \times R_{epic}) - (\kappa_{0\_ROT\_bore}(\theta) + \kappa_R \times R_{epic}) \\ &= \Delta\kappa_{0\_ROT}(\theta)\end{aligned} \tag{5}$$

It should be noted that errors in the azimuth of borehole sensors (i.e., sensors not oriented in the true NS or EW directions) could propagate through the estimation of $\Delta\kappa(\theta)$, which means that values of θ at the surface and at depth may not be consistent. The errors in the azimuth are observed at eight selected sites, and the maximum borehole sensor deflection is 4° (shown in Table 1). Thus, we correct the borehole record orientation with the azimuth of borehole sensors provided by Hi-net before the borehole horizontal component is rotated.

5. Results and Discussion

5.1. Directionality effects on κ_r and κ_0 estimations

A variation of $\kappa_{r\_AS\_ROT}$ with rotation angle is observed for both surface and borehole records at all stations. **Figure 5** presents an example of the relationship between $\kappa_{r\_AS\_ROT}$ and rotation angles at FKSH19. The corresponding FAS of the rotated components are also presented (i.e., with rotation angle of 80^o and 160^o) for comparison purposes, depicting changes of the decay in the high-frequency range. The standard derivations corresponding to $\kappa_{r\_AS\_ROT\_sur}$, and $\kappa_{r\_AS\_ROT\_bore}$ are 0. 0109 s and 0.0041 s, respectively.

Figure 5 illustrates that the variation of $\kappa_{r\_AS\_ROT}$ at the surface is more significant than at depth, which is also observed for the majority of records across all stations. We then investigate the influence of the event azimuth on the maximum $\kappa_{r\_AS\_ROT}$ observed and its corresponding rotation angle. The rotation angle associated with the maximum $\kappa_{r\_AS\_ROT}$ is hereafter referred to as θ_{max}. A correlation between θ_{max} and the azimuth of each record at the surface and at depth is not found.

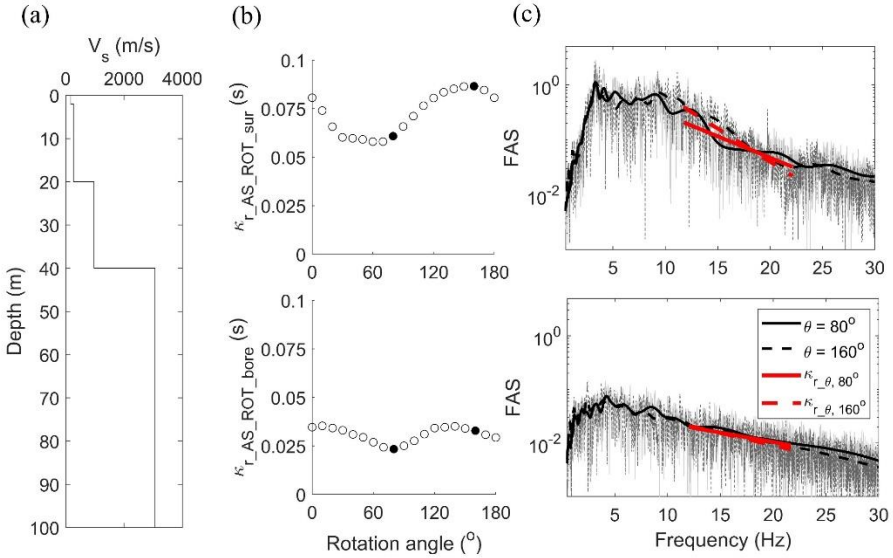

Figure 5. Example of $\kappa_{r\_AS\_ROT}$ variations. (a) Shear wave velocity profile at FKSH19, (b) comparison between $\kappa_{r\_AS\_ROT}$ and rotation angle at surface and borehole for one record, and (c) the FAS for rotated components with θ of 80^o and 160^o. The dark solid and dash lines show the smoothen FAS to emphasize the differences between rotated FASs. The select ground motion was a shallow active crustal event recorded at FKSH19 (site class: D) with seismic moment magnitude of 4.4, azimuth of 19^o, and epicentral distance of 117 km (recorded on 07/26/2003 (UT)).

The mean of all $\kappa_{r\_AS\_ROT}$ for each record, $\kappa_{r\_AS\_mean}$, and the average of $\kappa_{r\_AS\_H1}$ and $\kappa_{r\_AS\_H2}$ from the corresponding as-recorded horizontal components, $\kappa_{r\_AS\_ave}$, are compared in **Figure 6** by means of the ratio, $r_2 = \kappa_{r\_AS\_ave} / \kappa_{r\_AS\_mean}$. **Figure 6** demonstrates that the differences between $\kappa_{r\_AS\_mean}$ and $\kappa_{r\_AS\_ave}$ values at the ground surface are small; the maximum average of surface r_2 across the ten study sites is 1.04 (at IBRH13; V_{s30} = 335 m/s) and the minimum average is 0.96 (at FKSH16; V_{s30} = 532 m/s). However, at station IBRH14 (V_{s30} = 829 m/s), the differences of borehole $\kappa_{r\_AS\_mean}$ and $\kappa_{r\_AS\_ave}$ values are relatively large, with an average r_2 of 0.85 and a standard derivation of r_2 equal to 0.19. A closer inspection of the empirical transfer function (ETF)

at this station reveals that κ_{r_AS} estimates at IBRH14 could be affected by the site-amplification in high frequencies, which can help explain observed differences between $\kappa_{r\_AS\_mean}$ and $\kappa_{r\_AS\_ave}$. The corresponding ETFs at IBRH13, FKSH08, FKSH16, and FKSH19 also show varying site-amplification in the high frequency range. Considering the similarity observed between values of $\kappa_{r\_AS\_mean}$ and $\kappa_{r\_AS\_ave}$ for multiple ground motions and across study sites, an orientation-independent κ_r value for one recorded event at a given station can be estimated from the average of $\kappa_{r\_AS\_H1}$ and $\kappa_{r\_AS\_H2}$ computed from as-recorded orthogonal horizontal components directly. In the following sections, we use $\kappa_{r\_AS\_ave}$ (also denoted as κ_{r_AS} for simplicity) as the representative value for each pair of orthogonal horizontal components.

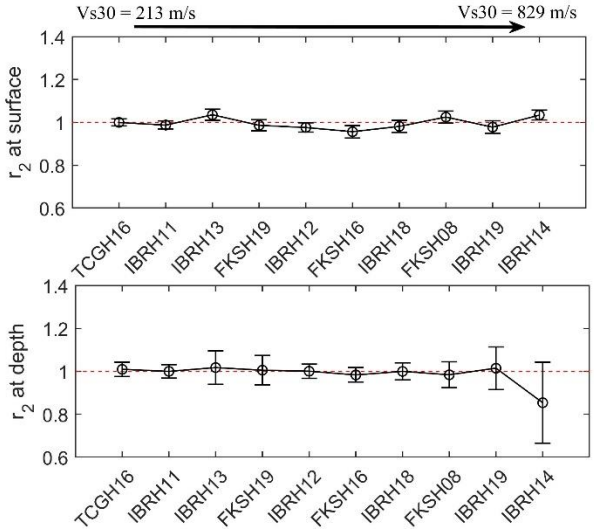

Figure 6. Comparison between mean κ_{r_AS} of rotated motions (i.e., $\kappa_{r\_AS\_mean}$) and mean κ_{r_AS} of two recorded horizontal component (i.e., $\kappa_{r\_AS\_ave}$) at selected stations along with the corresponding standard derivation at (a) borehole and (b) ground surface. r_2 corresponds to the ratio $\kappa_{r\_AS\_ave}/\kappa_{r\_AS\_mean}$. The dash line indicates an r_2 equal to 1.0, and the circles depict the mean r_2 across all records considered per station. The error bars indicate the +/- standard deviation of all r_2 computed at each site of interest.

The effects of ground motion directionality on $\Delta\kappa(\theta)$ (Equation (5)) are also explored to investigate how the orientation of ground motion can affect the seismic attenuation taking place throughout the soil column. **Figure 7** and **Table** 2 show the variations of $\Delta\kappa(\theta)$ at the sites of interest. First, we observe that the seismic attenuation contributed by the soil column is affected by ground motion directionality. Second, there seems to be a systematic variation with directionality unique to each site, with the maximum $\Delta\kappa(\theta)$ generally corresponding to the same rotation angle across different ground motions at each station. Kotha et al. (2019) proved that the contribution of radiation pattern to the ground shaking characteristics would be weak and random in the high frequency range. Thus, we hypothesize that the influence of ground motion directionality on the high-frequency parameter κ is station-dependent and not affected by the earthquake source. Moreover, the maximum σ for $\Delta\kappa(\theta)$ is observed at FKSH16, which has a thick soil column (hole-depth of 300 m, and H_{800} = 180 m) and a V_{s30} = 532 m/s. The minimum σ value is found at IBRH19 with H_{800} of 2 m, V_{s30} of 692 m/s and hole-depth of 210 m. However, a strong correlation between σ and H_{800} or V_{s30} or hole depth is not evident across all study sites. Different site parameters (or

a combination of existing ones) with considerations of shallow and deeper geologic structures are required to further detect potential correlations between site conditions and variability in $\Delta\kappa_0$ due to ground motion directionality.

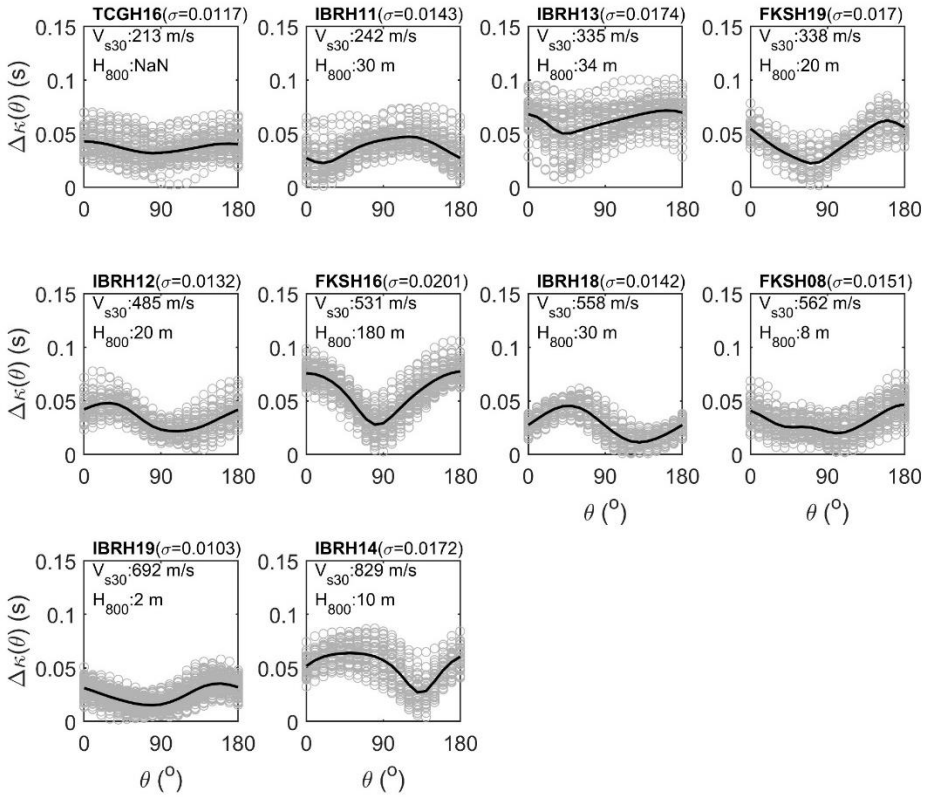

Figure 7. Variability of $\Delta\kappa(\theta)$ at the stations of interest and the corresponding site information. The solid lines represent the mean of all $\Delta\kappa(\theta)$ across all records per rotation angle, while the gray circles depict $\Delta\kappa(\theta)$ obtained for each record and multiple rotation angles. H_{800} refers to depth to a horizon with velocity V_s of 800 m/s or more.

Finally, we compare the mean of all $\Delta\kappa(\theta)$ values with the difference between surface and borehole κ_0 values (hereafter referred to as $\Delta\kappa_0$) from empirical linear regressions conducted on as-recorded horizontal components (i.e., averaging as-recorded κ_{r_AS} values for each pair) at each station (**Figure 8**). Mean values of $\Delta\kappa(\theta)$ shown in **Figure 8** are only slightly higher than the corresponding $\Delta\kappa_0$ values, which indicates that the mean of two as-recorded κ_{r_AS} values can lead to an orientation-independent estimation of $\Delta\kappa_0$. **Figure 8** also provides a comparison of the within-station and between-station variability of $\Delta\kappa(\theta)$. For most stations considered in this study (i.e., FKSH08, IBRH14, IBRH12, FKSH19, IBRH18, IBRH13 and IBRH11), the within-station variability in $\Delta\kappa(\theta)$ is comparable and sometimes more significant, which evidences the need for a more rigorous consideration of the within-station variability in κ_0 estimates. We note that the observed larger within-station variabilities in $\Delta\kappa(\theta)$ at IBRH13, IBRH14, FKSH08, and FKSH19 can be influenced by site-amplification effects at these sites in the high frequency. The latter can induce bias in the resulting κ values. The quantification of the within-station variability in κ will result in more reliable κ_0 estimates, which can inform empirical correlations with local site conditions.

Table 2. Station information and statistical parameters for $\Delta\kappa(\theta)$

Station Name	*Hole Depth	†H_{800}	††$V_{s,mean}$	§$\sigma(\Delta\kappa(\theta))$	‖mean($\Delta\kappa(\theta)$)	**NEHRP Site Class
	m	m	m/s	s	s	
IBRH14	100	10	1601.44	0.0172	0.0525	B
IBRH19	210	2	1792.68	0.0103	0.0249	C
FKSH08	105	8	936.59	0.0151	0.0310	C
IBRH18	504	30	1522.67	0.0142	0.0279	C
FKSH16	300	180	841.95	0.0201	0.0566	C
IBRH12	200	20	967.53	0.0132	0.0341	C
FKSH19	100	20	842.76	0.0170	0.0422	D
IBRH13	100	34	793.95	0.0174	0.0620	D
IBRH11	103	30	649.92	0.0143	0.0366	D
TCGH16	112	NaN	369.34	0.0138	0.0369	D

*Hole-depth: the depth of borehole sensor relative to the ground surface

†H_{800}: depth to a horizon with velocity V_s of 800 m/s or more

††$V_{s,mean}$: the time-averaged shear-wave velocity of the subsoil between surface and borehole sensors

§$\sigma(\Delta\kappa(\theta))$: standard derivation of $\Delta\kappa(\theta)$, which is computed with Equation (5)

‖mean($\Delta\kappa(\theta)$): mean of $\Delta\kappa(\theta)$, which is computed with Equation (5)

**NEHRP Site Class: National Earthquake Hazards Reduction Program (NEHRP) site class classification

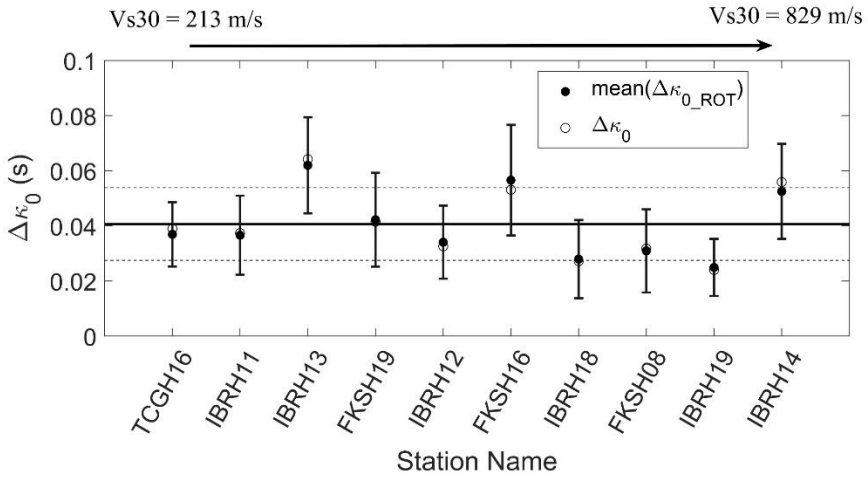

Figure 8. Comparison of mean($\Delta\kappa(\theta)$) and $\Delta\kappa_0$ at each station. $\Delta\kappa_0$ is the difference between surface and borehole κ_0 estimated from empirical regressions on as-recorded horizontal components. The error bar (within-station variability) represents ±1 standard derivation of $\Delta\kappa(\theta)$ at each station. The horizontal solid line presents the mean of $\Delta\kappa(\theta)$ across all stations, and the

dash lines indicate the ±1 standard derivation of $\Delta\kappa(\theta)$ across all considered stations (between-station variability).

5.2. Earthquake type and focal depth effects on κ_r, κ_R, and κ_0 estimations

In this section, we investigate the influence of earthquake type and focal depth on average κ_{r_AS} from as-recorded components, regional attenuation, as captured by κ_R, and κ_0 estimations. The algorithm proposed by Garcia et al. (2012) is used herein to classify earthquake types as: (1) shallow active crustal, ACRsh (if the hypocentral depth is less than 35 km), (2) deep active crustal, ACRde (if the hypocentral depth is larger than 35 km), (3) subduction zone intraslab, SZintra (with minimum focal depth of 15 km), and (4) subduction zone interface, SZinter, earthquakes (with minimum focal depth of 70 km).

Values of $\Delta\kappa_0$, κ_{0_sur}, κ_{0_bore}, and κ_R at the selected ten stations are computed for different datasets categorized by earthquake type, and shown in **Figure 9**. It should be noted that the limited number of ACRde events did not allow for the derivation of the corresponding κ_0 and κ_R for this particular dataset. A few negative values of κ_R and κ_0 values are obtained at some stations for some of the datasets, which could be caused by the lack of available events for each earthquake type at specific epicentral distance ranges. For example, ACRsh events recorded at IBRH11 only have epicentral distances in the range of 50 to 150 km. Hence, those cases were not included in **Figure 9**. The resulting κ_0 and κ_R values demonstrate that different seismicity types lead to varying estimates of the κ_R component (i.e., the slope of κ_0-model), which in turn affects the estimated site-specific κ_0 component (i.e., the intersect in the y-axis at zero epicentral distance). Records from subduction and active crustal earthquakes will be affected by different wave propagation paths, which is reflected in the variability in the path-component κ_R. Variations in $\Delta\kappa_0$ values at selected stations are relatively small for the different datasets considered, which supports previous research indicating the site-specific nature of $\Delta\kappa_0$ values that is not affected by the focal depth (i.e., the difference between κ_{0_sur} and κ_{0_bore} represents the seismic attenuation taking place throughout the local soil column, Cabas et al. 2017).

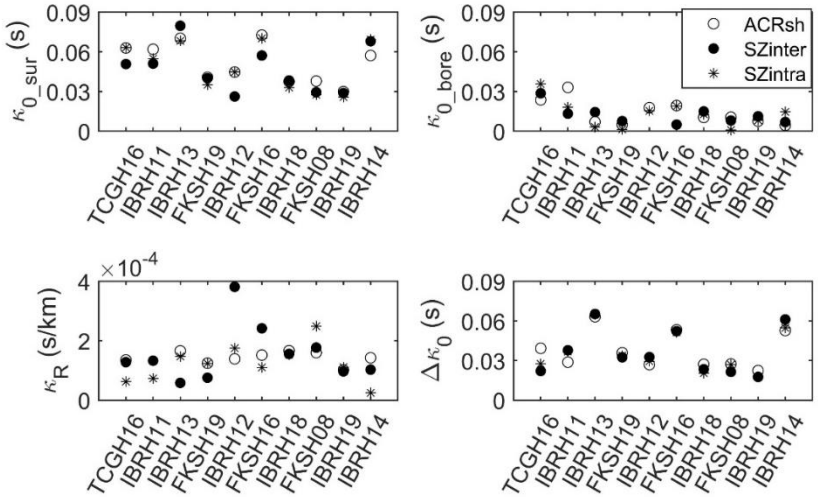

Figure 9. Comparisons of κ_0 (at the ground surface and at depth), κ_R, and $\Delta\kappa_0$ values for different earthquake types at each station.

The influence of focal depth on the estimations of κ_0 and κ_R is investigated by separating into three groups with focal depths of: (1) less than 35 km (which includes both ACRsh and SZintra events), (2) from 35 km to 70 km (which includes the ACRde and SZintra events), and (3) more than 70 km (which includes the ACRde and SZinter events). A correlation between κ_R values and focal depth is not observed, but κ_R values show less variation when grouped by focal depth (regardless of earthquake type) than by earthquake type as seen in **Figure 10**.

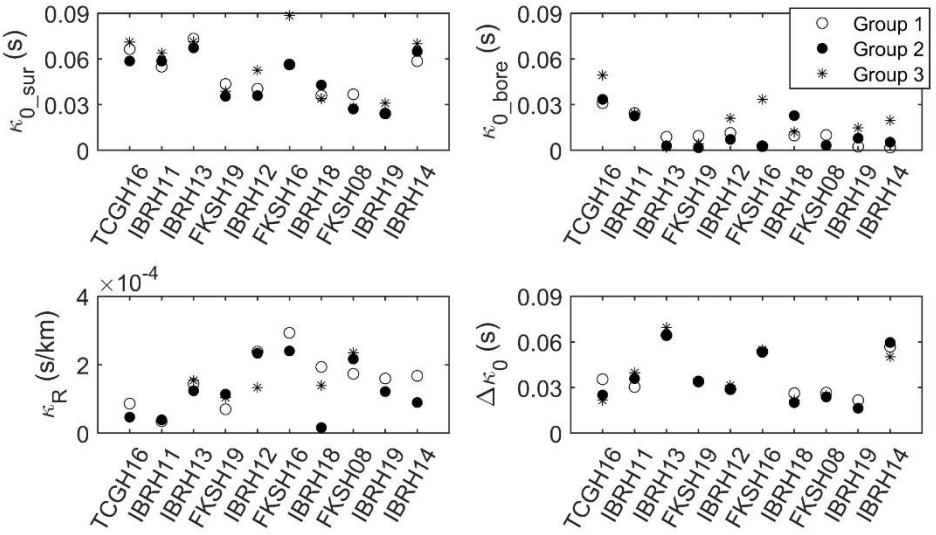

Figure 10. Comparisons of κ_0 (at the ground surface and at depth), κ_R, and $\Delta\kappa_0$ (the difference between surface and borehole κ_0) values for different focal depth groups at each station. Groups 1, 2 and 3 consider focal depths of less than 35 km, from 35 to 70 km, and more than 70 km, respectively.

The influence of earthquake type and focal depth is further explored in **Figure 11**, where κ_R, κ_0 and $\Delta\kappa_0$ values estimated only using ACRsh events, and a dataset of records with focal depth less than 35 km (i.e., Group 1) are compared. It should be noted that a negative κ_R value is derived at IBRH11 for the ACRsh datasets, which may be caused by the absence of events for epicentral distance less than 50 km. The average differences of κ_R estimations between these two data sets across the ten stations is 28.43% (neglecting the values at IBRH11), while the corresponding average differences of κ_{0_sur} and $\Delta\kappa_0$ are 8.77% and 4.51%, respectively. The differences in κ_R, κ_{0_sur}, κ_{0_bore}, *and* $\Delta\kappa_0$ estimates are acceptable, which supports the incorporation of shallow subduction zone events to a shallow crustal event dataset.

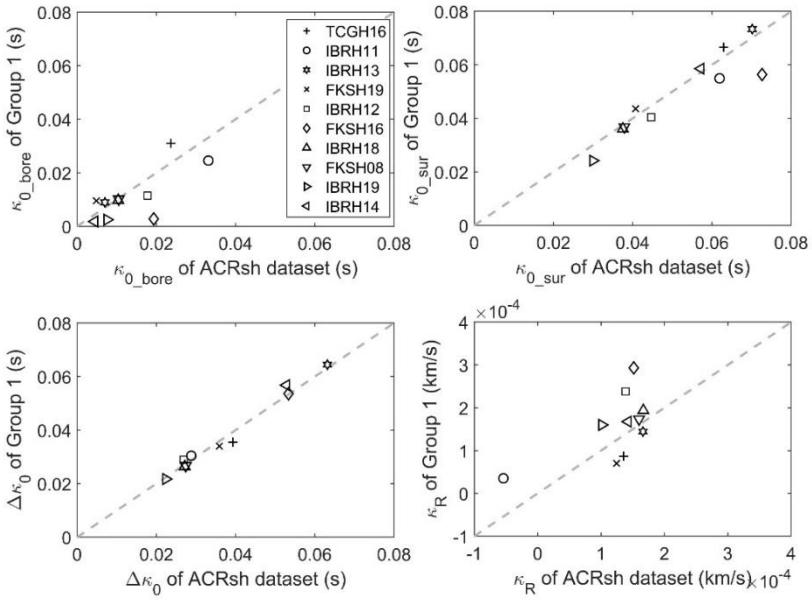

Figure 11. Comparisons of κ_0 (at the ground surface and at depth), κ_R, and $\Delta\kappa_0$ (the difference between surface and borehole κ_0) values estimated with ACRsh dataset, and Group 1. Group 1 includes the events with focal depth less than 35 km (which includes both ACRsh and SZintra events).

6. Conclusions

Repeatable contributions from path and site terms to the within-station variability in individual estimates of κ_r and site-specific κ_0 were investigated using ten stations from the KiK-net database. Our dataset consisted of linear ground motions with surface PGA less than 0.01 g, M_w larger than 4.0 and epicentral distance less than 150 km. Both active crustal and subduction earthquakes were used in this work to investigate repeatable contributions from the wave propagation path. Systematic variability on κ_r and κ_0 values stemming from the dataset choice, namely the selection of events based on their focal depth and type of seismicity was evaluated. Contributions to the within-station variability associated with ground motion directionality were also investigated.

The influence of ground motion directionality on the estimates of κ_{r_AS} was studied, and findings from this work revealed that the orientation of ground motion affects estimates of κ_{r_AS} computed on single horizontal components. However, this influence can be removed when calculating the average of two as-recorded horizontal component κ_{r_AS} values. Thus, using the mean of two horizontal κ_{r_AS} values (without considerations of the difference between these two values) is recommended as the representative κ value for each ground motion pair. This is different from previous recommendations to only report κ_{r_AS} values for which differences between the recorded horizontal components is less than 20%. It was also found that the within-station variability in $\Delta\kappa_0$ values (i.e., the difference between κ_0 values at the surface and at depth) associated with directionality effects can be comparable to the between-station variability. This observation highlights the importance of quantifying the within-station variability on κ estimates in a more robust manner. Moreover, our findings support previous research efforts indicating that site

amplification effects on κ estimates should be minimized in order to obtain reliable estimates at sites of interest. Systematic contributions from event-azimuths were not observed, while the variability in $\Delta\kappa(\theta)$ estimates with rotation angle was found to be a function of local soil conditions. The influence of ground motion directionality on the parameterization of near-surface attenuation was found to be station-dependent, but further investigation is required to identify relevant correlations between observed ground motion directionality and site properties. Near-surface seismic attenuation anisotropy could help explain observed variations of $\Delta\kappa(\theta)$ with ground motion orientation. Anisotropy in Q values has been observed from both laboratory experiments (Tao and King, 1990, Kern et al. 1997) and the analysis of earthquake ground motions (Liu et al. 2005). The random distributed cracks near surface could also cause seismic anisotropy (Liu et al. 1993, Liu et al. 2004, Boness and Zoback 2004), which could then influence seismic wave scattering and reflection. The specific geological condition and volcanic environment in Japan also lead to anisotropy in Q (Pei et al. 2009, and Nakano et al. 2015). More generally, a preferred direction of ground motion independent from the expected polarization (based on focal mechanism and location of the events) has also been observed in recorded data from the Whittier Narrows and Loma Prieta earthquakes (Bonamassa et al. 1991, Bonamassa and Vidale 1991). More research on directionality effects is required to elucidate the physical basis for the observed variation of attenuation characteristics of ground motions with orientation.

Different earthquake types were found to lead to different κ_R values. However, it is important to note that the classification of seismicity type is also tied to the focal depth. Selecting a dataset with considerations of systematic variations stemming from varying focal depths and earthquake types is recommended to resolved κ's path-component, κ_R more reliably. Deep earthquakes can produce multi-wave propagation paths to the site of interest, which could have a more significant influence on κ_R. On the other hand, the incidence angle of seismic waves when the focal depth is shallow could introduce larger within-station variability. Smaller differences in surface and borehole κ_0 values were observed across the datasets used (i.e., different focal depths and/or earthquake types). The lack of variability of $\Delta\kappa_0$ values as a function of source and path effects evidences that $\Delta\kappa_0$ is mainly a function of near-surface attenuation, which supports its site-specific nature also observed in previous research studies.

7. Data and Resources

Accelerograms and geotechnical data are obtained from the KiK-net network at http://www.kyoshin.bosai.go.jp (last accessed December 2018), collected and distributed by National Research Institute for Earth Science and Disaster Prevention (NIED). The orientations of borehole sensors are available at http://www.hinet.bosai.go.jp/st_info/detail/?LANG=ja (last accessed December 2018). The earthquake information is available F-net network at http://www.fnet.bosai.go.jp/top.php (last accessed December 2018).

8. Acknowledgements

We appreciate that the National Research Institute for Earth Science and Disaster Prevention (NIED) provides the data for this work. We acknowledge Dr. Haitham Dawood and Dr. Adrian Rodriguez-Marek for providing their processed dataset. We are thankful to Associate Editor Martin Chapman, Benjamin Edwards, and one anonymous reviewer for the useful comments. This

study was sponsored by the U.S. Geological Survey under Grant No. G18AS00058. The views and conclusions contained in this document are those of the authors and should not be interpreted as representing the opinions or policies of the U.S. Geological Survey.

9. References

Anderson, J. G., & Hough, S. E. (1984). A model for the shape of the Fourier amplitude spectrum of acceleration at high frequencies. *Bull Seismol Soc Am*. **74**, no. 5, 1969-1993.

Anderson, J.G. (1991). A preliminary descriptive model for the distance dependence of the spectral decay parameter in southern California. *Bull Seismol Soc Am*. **81**, no. 6, 2186-2193.

Atik, L.A., Abrahamson, N., Bommer, J.J., Scherbaum, F., Cotton, F. and Kuehn, N., (2010). The variability of ground-motion prediction models and its components. *Seismol Res Lett*. **81**, no. 5, 794-801.

Al Atik, L., Kottke, A., Abrahamson, N. and Hollenback, J., (2014). Kappa (κ) scaling of ground-motion prediction equations using an inverse random vibration theory approach. *Bull Seismol Soc Am*, 104, no. 1, 336-346.

Aoi, S., T. Kunugi, and H. Fujiwara (2004). Strong-motion seismograph network operated by NIED: K-NETand KiK-net, *J. Japan Assoc. Earthq.Eng.* **4**, no. 3, 65–74.

Aoi, S., T. Kunugi, H. Nakamura, and H. Fujiwara (2011). Deployment of new strong motion seismographs of K-NET and KiK-net, *Geotech. Geol. Earthq. Eng*. **14**, 167–186, doi: 10.1007/978-94-007-0152-6_12.

Baltay, A.S., Hanks, T.C. and Abrahamson, N.A., (2017). Uncertainty, variability, and earthquake physics in ground-motion prediction equations. *Bull Seismol Soc Am,* **107**, no. 4, 1754-1772.

Biasi, G. P., and K. D. Smith (2001). Site Effects for Seismic Monitoring Stations in the Vicinity of Yucca Mountain, Nevada, MOL20011204.0045, a report prepared for the US DOE/ University and Community College System of Nevada (UCCSN) Cooperative Agreement.

Boness, N., and M. D. Zoback (2004). Stress-induced seismic velocity anisotropy and physical properties in the SAFOD pilot hole in Parkfield, CA., *Geophys. Res. Lett*., **31**. L15S17, doi:10.1029/2004GL019020

Brune, J. N. (1970). Tectonic stress and the spectra of seismic shear waves from earthquakes. *J Geophys Res*. **75**, no. 26, 4997-5009.

Brune, J. N. (1971). Correction to "Tectonic stress and the spectra of seismic shear waves from earthquakes," *J Geophys Res*. **76**, 5002.

Boore, D. M., Watson-Lamprey, J., & Abrahamson, N. A. (2006). Orientation-independent measures of ground motion. *Bull Seismol Soc Am.* **96**, no. 4A, 1502-1511.

Boore, D. M. (2010). Orientation-independent, nongeometric-mean measures of seismic intensity from two horizontal components of motion. *Bull Seismol Soc Am*. **100**, no. 4, 1830-1835.

Bommer, J.J. and Abrahamson, N.A., (2006). Why do modern probabilistic seismic-hazard analyses often lead to increased hazard estimates? *Bull Seismol Soc Am*. **96**, no. 6, 1967-1977.

Bonamassa, O. and Vidale, J.E., (1991). Directional site resonances observed from aftershocks of the 18 October 1989 Loma Prieta earthquake. *Bull Seismol Soc Am*. **81**, no. 5, 1945-1957.

Bonamassa, O., Vidale, J.E., Houston, H. and Schwartz, S.Y., (1991). Directional site resonances and the influence of near-surface geology on ground motion. *Geophys Res Lett*. **18**, no.5, 901-904.

Campbell, K.W., (2003). Prediction of strong ground motion using the hybrid empirical method and its use in the development of ground-motion (attenuation) relations in eastern North America. *Bull Seismol Soc Am*., 93, no.3, 1012-1033.

Campbell, K.W., (2009). Estimates of shear-wave Q and κ0 for unconsolidated and semiconsolidated sediments in Eastern North America. *Bull Seismol Soc Am*. **99**, no.4, 2365-2392.

Cabas, A. and Rodriguez-Marek, A., (2017). VS-κ 0 Correction Factors for Input Ground Motions Used in Seismic Site Response Analyses. *Earthquake Spectra*, **33**, no. 3, 917-941.

Cabas, A., Rodriguez-Marek, A., & Bonilla, L. F. (2017). Estimation of Site-Specific Kappa (κ0)-Consistent Damping Values at KiK-Net Sites to Assess the Discrepancy between Laboratory-Based Damping Models and Observed Attenuation (of Seismic Waves) in the Field. *Bull Seismol Soc Am*. **107**, no. 5, 2258-2271.

Dawood, H. M., Rodriguez-Marek, A., Bayless, J., Goulet, C., & Thompson, E. (2016). A flatfile for the KiK-net database processed using an automated protocol. *Earthquake Spectra*, **32**, no. 2, 1281-1302.

Douglas, J., Gehl, P., Bonilla, L.F. and Gélis, C., (2010). A κ model for mainland France. *Pure Appl Geophys.* **167**, no.11, 1303-1315.

Dimitriu, P., Theodulidis, N., Hatzidimitriou, P., & Anastasiadis, A. (2001). Sediment non-linearity and attenuation of seismic waves: a study of accelerograms from Lefkas, western Greece. *Soil Dynam Earthquake Eng*. **21**, no.1, 63-73.

Drouet, S., Cotton, F. and Guéguen, P., (2010). v S 30, κ, regional attenuation and M w from accelerograms: application to magnitude 3–5 French earthquakes. *Geophys J Int.* **182**, no. 2, 880-898.

Edwards, B., Ktenidou, O.J., Cotton, F., Abrahamson, N., Van Houtte, C. and Fäh, D., (2015). Epistemic uncertainty and limitations of the κ 0 model for near-surface attenuation at hard rock sites. *Geophys J Int.* **202**, no. 3, 1627-1645.

Fujiwara, H., S. Aoi, T. Kunugi, and S. Adachi (2004). Strong-motion observation networks of NIED: K-NETand KiK-net, National Research Institute for Earth Science and Disaster Prevention.

Garcia, D., Wald, D. J., & Hearne, M. G. (2012). A global earthquake discrimination scheme to optimize ground-motion prediction equation selection. *Bull Seismol Soc Am*. **102**, no.1, 185-203.

Kern, H., Liu, B. and Popp, T., (1997). Relationship between anisotropy of P and S wave velocities and anisotropy of attenuation in serpentinite and amphibolite. *J Geophys Res: Solid Earth*, **102**, no.B2, 3051-3065.

Kuehn, N.M., Abrahamson, N.A. and Walling, M.A., (2019). Incorporating Nonergodic Path Effects into the NGA-West2 Ground-Motion Prediction Equations. *Bull Seismol Soc Am*. **109**, no.2, 575-585.

Knopoff, L., (1964). Q. *Rev. Geophysics*, 2, no. 4, 625-660.

Ktenidou, O. J., Gélis, C., & Bonilla, L. F. (2013). A study on the variability of kappa (κ) in a borehole: Implications of the computation process. *Bull Seismol Soc Am*. **103**, no.2A, 1048-1068.

Ktenidou, O. J., Cotton, F., Abrahamson, N. A., & Anderson, J. G. (2014). Taxonomy of κ: A review of definitions and estimation approaches targeted to applications. *Seismol Res Lett*. **85**, no.1, 135-146.

Ktenidou, O.J., Abrahamson, N.A., Drouet, S. and Cotton, F., (2015). Understanding the physics of kappa (κ): Insights from a downhole array. *Geophys J Int.* **203**, no. 1, 678-691.

Ktenidou, O.J., Abrahamson, N., Darragh, R. and Silva, W., (2016). A methodology for the estimation of kappa (κ) from large datasets, example application to rock sites in the NGA-East database, and implications on design motions. PEER Report 2016, 1.

Kotha, S.R., Cotton, F. and Bindi, D., (2019). empirical Models of shear-Wave Radiation pattern Derived from Large Datasets of Ground-shaking observations. *Scientific reports*, 9, no.1, 1-11.

Laurendeau, A., Cotton, F., Ktenidou, O. J., Bonilla, L. F., & Hollender, F. (2013). Rock and stiff-soil site amplification: Dependency on VS 30 and kappa (κ 0). *Bull Seismol Soc Am*. **103**, no. 6, 3131-3148.

Liu, E., Crampin, S., Queen, J.H. and Rizer, W.D., (1993). Velocity and attenuation anisotropy caused by microcracks and macrofractures in a multiazimuth reverse VSP. *Can. J. Explor. Geophys*. **29**, no. 1, 177-188.

Liu, Y., Teng, T.L. and Ben-Zion, Y., (2004). Systematic analysis of shear-wave splitting in the aftershock zone of the 1999 Chi-Chi, Taiwan, earthquake: shallow crustal anisotropy and lack of precursory variations. *Bull Seismol Soc Am*. **94**, no.6, 2330-2347.

Liu, Y., Teng, T.L. and Ben-Zion, Y., (2005). Near-surface seismic anisotropy, attenuation and dispersion in the aftershock region of the 1999 Chi-Chi earthquake. *Geophys J Int.* **160**, no. 2, 695-706.

Mayor, J., Bora, S. S., & Cotton, F. (2018). Capturing Regional Variations of Hard-Rock κ 0 from Coda Analysis. *Bull Seismol Soc Am*.**108**, no. 1, 399-408.

Nakano, K., Matsushima, S., & Kawase, H. (2015). Statistical properties of strong ground motions from the generalized spectral inversion of data observed by K-NET, KiK-net, and the JMA Shindokei network in Japan. *Bull Seismol Soc Am*.**105**, no. 5, 2662-2680.

Oth, A., Parolai, S. and Bindi, D., (2011). Spectral analysis of K-NET and KiK-net data in Japan, Part I: Database compilation and peculiarities. *Bull Seismol Soc Am*. **101**, no.2, 652-666.

Pei, S., Cui, Z., Sun, Y., Toksöz, M. N., Rowe, C. A., Gao, X., & Morgan, F. D. (2009). Structure of the upper crust in Japan from S-wave attenuation tomography. *Bull Seismol Soc Am*. **99**, no. 1, 428-434.

Parolai, S. and Bindi, D., (2004). Influence of soil-layer properties on k evaluation. *Bull Seismol Soc Am*, 94, no.1, 349-356.

Parolai, S., Bindi, D. and Pilz, M., (2015). k 0: The role of Intrinsic and Scattering Attenuation. *Bull Seismol Soc Am*. **105**, no. 2A, 1049-1052.

Parolai, S., (2018). κ 0: Origin and Usability. *Bull Seismol Soc Am*.**108**, no. 6, 3446-3456.

Perron, V., Hollender, F., Bard, P. Y., Gélis, C., Guyonnet-Benaize, C., Hernandez, B., & Ktenidou, O. J. (2017). Robustness of kappa (κ) measurement in low-to-moderate seismicity areas: Insight from a site-specific study in Provence, France. *Bull Seismol Soc Am*. **107**, no.5, 2272-2292.

Pilz, M. and Fäh, D., (2017). The contribution of scattering to near-surface attenuation. *Journal of Seismology*, **21**, no. 4, 837-855.

Pilz, M. and Cotton, F., (2019). Does the 1D assumption hold for site response analysis? A study of seismic site responses and implication for ground motion assessment using KiK-net strong-motion data. *Earthquake Spectra*, **35**, no.2, 883-905.

Pilz, M., Cotton, F., Zaccarelli, R. and Bindi, D., (2019). Capturing Regional Variations of Hard-Rock Attenuation in Europe. *Bull Seismol Soc Am*, 109, no.4, 1401-1418.

Rodriguez-Marek, A., Rathje, E.M., Bommer, J.J., Scherbaum, F. and Stafford, P.J., (2014). Application of single-station sigma and site-response characterization in a probabilistic seismic-hazard analysis for a new nuclear site. *Bull Seismol Soc Am*. **104**, no.4, 1601-1619.

Silva, W. J., and R. Darragh (1995). Engineering Characterization of Earthquake Strong Ground Motion Recorded at Rock Sites, Palo Alto, Electric Power Research Institute, TR-102261.

Tao, G., and M. S. King (1990). Shear-wave velocity and Q anisotropy in rocks: A laboratory study, *Int. J. Rock Mech. Min. Sci. Geomech. Abstr.* **27**, 353–361.

Van Houtte, C., Drouet, S., & Cotton, F. (2011). Analysis of the origins of κ (kappa) to compute hard rock to rock adjustment factors for GMPEs. *Bull Seismol Soc Am*.**101**, no. 6, 2926-2941.

Van Houtte, C., Ktenidou, O.J., Larkin, T. and Holden, C., (2014). Hard-site κ 0 (kappa) calculations for Christchurch, New Zealand, and comparison with local ground-motion prediction models. *Bull Seismol Soc Am*.**104**, no. 4, 1899-1913.

Xu, B., Rathje, E.M., Hashash, Y., Stewart, J., Campbell, K. and Silva, W.J., (2019). κ 0 for Soil Sites: Observations from Kik-net Sites and Their Use in Constraining Small-Strain Damping Profiles for Site Response Analysis. *Earthquake Spectra*. 36, no.1, 111-137.

Wu H. Masaki K. Irikura K., and Sánchez-Sesma F. J. (2017). Application of a simplified calculation for full-wave microtremor H/V spectral ratio based on the diffuse field approximation to identify underground velocity structures, Earth Planets Space 69, no. 1, 162

Part II: Quantifying the High-frequency Spectral Decay Parameter Kappa (κ) Beyond the Linear-elastic Regime

1. Introduction

The anelastic attenuation of seismic waves as they travel through sedimentary deposits is a function of the deformations induced, which in turn depends on the material properties (e.g., plasticity of the soil) and the intensity of the ground shaking. Material damping ratio, ξ, is commonly used in geotechnical earthquake engineering to quantify viscous and anelastic energy dissipation in soils subjected to dynamic loading. Empirical models of ξ often have a constant minimum value (known as minimum shear-strain damping, ξ_{min}) for small shear strains considered in the linear-elastic regime (e.g., Darendeli, 2001). Yet values of ξ increase as larger shear strains are induced in soil deposits by stronger ground excitations (Idriss et al. 1978, Seed et al. 1986, Darendeli 2001). The characterization of ξ across a wide range of strains is essential to model the effects of local soil conditions on earthquake ground motions.

The high-frequency spectral decay parameter, κ (Anderson and Hough 1984) is based on characteristics of low-intensity ground motions recorded directly in the field, which makes it an observable parameter that quantifies total attenuation (e.g., energy dissipation caused by scattering and anelasticity). Estimates of κ have proven useful in multiple applications, from stochastic modeling of ground motions (Boore 2003) to the development of host-to-target adjustments of ground motion models (e.g., Campbell 2003, Al Atik et al. 2014). The site-specific, distance-independent component of κ, known as κ_0 (Anderson 1991) is defined as a site parameter that captures the attenuation due to the propagation of seismic waves through near-surface materials. The relationship between κ_0 and ξ_{min} has been investigated in previous studies (e.g., Cabas et al. 2017; Ktenidou et al. 2015; Zalachoris and Rathje 2015) for weak motion data, but the quantification of κ and κ_0 beyond the linear-elastic regime remains unsolved.

Most studies on individual estimates of κ, hereafter referred to as κ_r, and its site-specific component κ_0 have used ground motion records that do not trigger nonlinear behavior at the sites of interest (e.g., Van Houtte et al. 2011, Laurendeau et al. 2013, Edwards et al. 2015, Perron et al. 2017). This practice is consistent with the concept of κ_r introduced by Anderson and Hough (1984), who associated the deviation from a flat high-frequency acceleration spectrum to attenuation along the path. However, nonlinear soil behavior has often been responsible for increasing the damage potential of strong ground motions in past earthquakes (e.g., Darragh and Shakal, 1991, Trifunac and Todorovska, 1994, Bonilla et al., 2011, Rong et al., 2016). Understanding near-surface attenuation effects in the nonlinear regime is then necessary for a thorough assessment of seismic hazards and risks imposed to civil infrastructure (Anderson and Hough 1984). Hence, this paper investigates the relationships among κ, shear strains and ground motion intensity to understand the behavior of κ at the onset of nonlinear soil behavior.

2. Background

The first paper that attempted to connect soils' nonlinear response and κ_r was conducted by Yu et al. (1992), where the authors compared two simulated records; one from a linear site response analysis, and the other from a time-domain nonlinear site response analysis. Yu et al. (1992) indicated that the value of κ_r estimated with the Anderson and Hough (1984) approach and corresponding to the motion affected by soil nonlinearity was smaller due to the nonlinear site amplifications at high frequencies. However, later studies found a positive correlation between κ_r (and κ_0), strain amplitudes and the intensity of ground shaking (e.g., Durward et al 1996; Lacave-Lachet et al 2000; Dimitriu et al. 2001; Van Houtte et al 2014).

Durward et al. (1996) found that κ_r values were a function of peak ground velocity (PGV, varying from 1 to 100 cm/s), which was used as a proxy for deformation. Values of κ_r were computed for more than 60 records observed at 23 sites in the Imperial Valley, California based on the acceleration spectrum approach (Anderson and Hough, 1984). Durward et al. (1996) hypothesized that soil nonlinearity had affected κ_r because higher κ_r values correlated well with higher PGVs. Moreover, Lacave-Lachet et al. (2000) analyzed ground motions from the 1995 Kobe earthquake in Japan (i.e., the main shock and aftershocks), and found that κ_r values increased with increasing peak ground acceleration (PGA). Hence, Lacave-Lachet et al. (2000) proposed to use κ_r to detect the onset of soil nonlinearity. Dimitriu et al. (2001) investigated the dependency between site-specific κ_0 and ground shaking intensity. Values of κ_r for 23 ground motions (i.e., 46 horizontal components with values of κ_r reported for each individual component) were computed at two adjacent sites in Lefkas, western Greece, based on the acceleration spectrum method. Dimitriu et al. (2001) provided evidence that κ_0 was a proxy for soil nonlinearity based on the observed dependency between κ_0 and ground shaking amplitudes, which were represented by mean horizontal acceleration in the S-wave window (MGA), PGA, and PGV. Positive correlations were found between the 46 κ_0 values and MGA, PGA, and PGV in log-scale, while a negative correlation was observed between κ_0 and the site dominant-resonance frequency. Similarly, Van Houtte et al. (2014) identified a positive correlation between estimates of κ_0 and PGA at soft sites using ground motions from the 2010-2011 Canterbury earthquake sequence in New Zealand.

There are still few and contradicting observations of the effects of nonlinearity on κ_r and κ_0 estimates (Ktenidou et al. 2015). Additionally, previous studies only considered a very limited database of ground motions. This paper takes advantage of the unique Japanese Kiban-Kyoshin network (KiK-net), which is rich in high-quality ground motions, to further investigate the effects of soil nonlinearity on κ_r and κ_0. More specifically, we explore the dependence of κ_r and κ_0 on ground shaking intensity (i.e., weak, moderate or strong ground motions) as parameterized by PGA, and on the level of shear strains induced in near-surface materials at 20 KiK-net stations. First, we present the conceptual basis for the relationship between κ, shear strains and ground motion intensity. Then, we describe our database and methods, starting with the identification of an appropriate classification scheme for linear and nonlinear regimes. The analysis of the effects of ground shaking amplitudes on κ_r at each study site follows. Lastly, we compare the ratio of nonlinear and linear site-specific κ_0 across all selected stations to assess the variation of near-surface attenuation estimates from the linear-elastic to the nonlinear regime.

3. Conceptual basis for the interpretation of κ beyond the linear-elastic regime

The induced strain level in a given soil layer is a function of the material properties, and the amplitude and frequency content of the incoming wavefield at the site. Stronger ground shaking results in larger-strain responses, which produce an increase in material damping ratio (in combination with a reduction of shear modulus). The short wavelength of high frequency waves allows for multiple cycles of shearing in near-surface sedimentary layers, which makes them more sensitive to the effects of a higher material damping ratio. Thus, we hypothesize that stronger ground shaking inducing larger deformations in sedimentary deposits will affect estimates of the high-frequency spectral decay parameter κ.

Figure 1 provides the acceleration Fourier amplitude spectrum (FAS) and empirical transfer function (ETF) corresponding to a pair of ground motions recorded at depth and at the ground surface at AICH17. One of the ground motion pairs has a low ground shaking intensity (with a surface PGA of less than 5 gals), while the other one has a higher ground shaking intensity (with a surface PGA greater than 40 gals). Computed FAS and ETF are provided for each horizontal component of the low- and high-intensity ground motion pairs in Figure 1. Individual κ_r values are provided for both pairs to explore the validity of our hypothesis with respect to changes in κ due to the intensity of ground shaking. To minimize the bias from path effects and isolate local site effects on individual κ_r values, the selected weak and strong ground motions correspond to events with similar focal depths, azimuths and epicentral distances (i.e., the focal depths, azimuths and epicentral distances are 5 km, 349.2^o, and 76.77 km, respectively for the low-intensity event, and 5 km, 350.5^o, and 76.95 km, respectively for the high-intensity event). The moment magnitudes of the events associated with the weak and strong ground motions in Figure 1 are 4.2 and 5.2, respectively. To reduce the variability associated with the calculation of κ_r from the acceleration spectrum method, we use the same frequency window for all ground motions (Edwards et al. 2011). Larger values of κ_r at the ground surface (i.e., 0.066 s for horizontal component H_1 and 0.070 s for horizontal component H_2) are obtained for the high-intensity ground motion compared to the corresponding κ_r values for the low-intensity ground motion (i.e., 0.059 s and 0.053 s for H_1 and H_2, respectively). The surface PGA values for the low-intensity record are 4.67 and 3.9 gals for H_1 and H_2, and for the high-intensity ground motion are 91.98 and 41.79 gals. Meanwhile, the ETF corresponding to the high-intensity event shows lower amplifications at higher frequencies (e.g., amplification of varies from 4.3 to 10.6 between 10 and 20 Hz for H_1) than its counterpart for the low-intensity ground motion (i.e., amplification varies from 4.8 to 17 between 10 and 20 Hz for H_1), which reflects the stronger influence of increased material damping ratio on high frequencies.

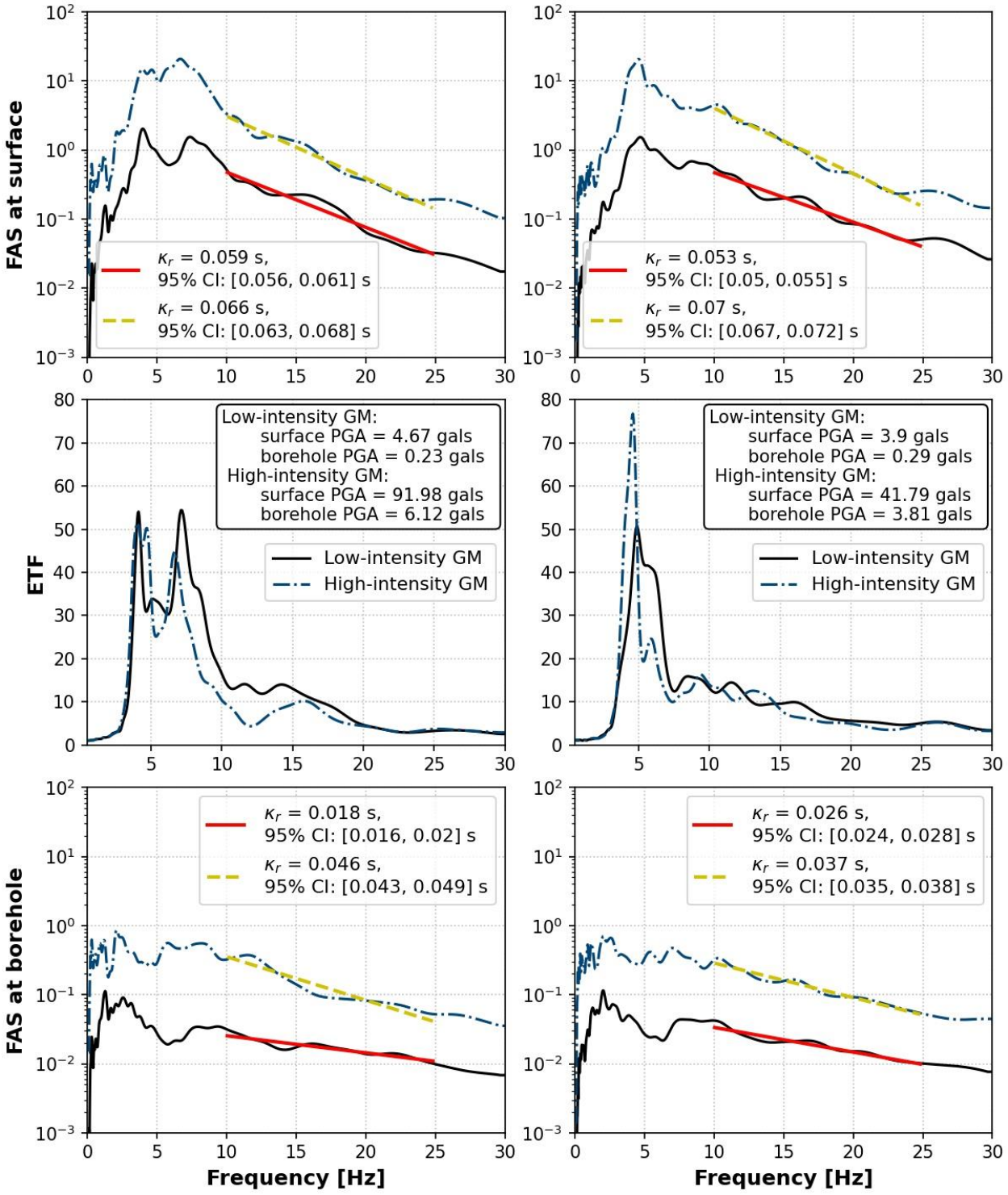

Figure 1. Comparisons between a weak and a strong ground motion recorded at AICH17 (V_{s30} = 314 m/s). The M_w and R_e are 4.2 and 76.77 km for the low-intensity ground motion, while 5.2 and 76.95 km for the high-intensity ground motion. The frequency window (i.e., [10, 25] Hz) applied in this plot are picked manually. The left and right columns correspond to analyses conducted on the horizontal components H_1 and H_2, respectively.

4. Database description

In this study, we use ground motions from the KiK-net database, which provides high quality strong ground motions recorded at more than 600 stations installed uniformly across Japan. Each station possesses a pair of sensors, one at the surface and another one at depth that is typically between 100 to 200 m deep. The sampling frequency of the observed acceleration series is either 100 or 200 Hz. The P- and S-wave velocity profiles are measured by downhole PS logging and available at the KiK-net website (see Resources and Data). The earthquake information, including the seismic moment magnitude M_w, focal depth and epicenter location are provided by the broadband seismography network (F-net) catalog. The ground motions and flatfile used in this work are processed with the automated protocol proposed by Bahrampouri et al. (2020).

We use surface and borehole horizontal records in this paper. The criteria applied to select records are as follows: (1) epicentral distance is less than 150 km, (2) the SNR ratio is larger than 3.0 at each frequency from 1.0 to 30 Hz, (3) focal depth is less than 35 km (Ji et al. 2020), and (4) the seismic wave path does not pass the Japanese volcanic belt (Nakano et al. 2015). Thus, twenty stations with more than five nonlinear ground motions (the definition of nonlinear ground motions is described next in the Methods section) are used in this work (with 18 stations having more than 10 nonlinear records and 8 stations having more than 15 nonlinear records, see Table 1). Table 1 provides local soil conditions and number of ground motions at each selected site and Figure 2 shows the corresponding locations of selected stations.

Table 1. Local soil conditions, number of ground motions per dataset, predetermined fixed-frequency bandwidth and thresholds for shear strain index, I_γ at all study sites.

Station	V_{s30}[1] (m/s)	V_{s0}[2] (m/s)	$V_{s,depth}$[3] (m/s)	Hole Depth (m)	Number of linear records	Number of transitional records	Number of nonlinear records	f_1[4] (Hz)	f_2[5] (Hz)	$I_{\gamma,0,l}$[6] (%)	$I_{\gamma,0,t}$[7] (%)
AICH17	314	150	2200	101	23	27	12	12.65	25.00	0.001	0.003
CHBH13	235	220	2920	1300	139	49	11	8.95	25.00	0.001	0.003
FKSH11	240	110	700	115	148	140	26	13.97	25.00	0.001	0.003
FKSH14	237	120	1210	147	114	221	28	10.05	25.00	0.001	0.007
FKSH18	307	140	2250	100	158	103	16	8.95	25.00	0.001	0.003
FKSH19	338	170	3060	100	185	95	21	10.05	25.00	0.001	0.003
FKSH21	365	200	1600	200	60	17	8	12.65	25.00	0.001	0.003
IBRH16	626	140	2050	300	137	81	15	10.05	25.00	0.001	0.003
IBRH17	301	90	2300	510	117	177	18	13.01	25.00	0.001	0.007
IBRH20	244	180	1200	923	133	86	11	8.95	25.00	0.001	0.007
IWTH21	521	150	2460	100	39	24	6	7.38	25.00	0.001	0.003
IWTH26	371	130	680	108	79	32	11	14.24	25.00	0.001	0.003
KMMH01	575	150	1900	100	94	24	15	13.97	25.00	0.001	0.003
KMMH12	410	210	1000	123	134	34	11	11.44	25.00	0.001	0.003
MYGH07	366	130	740	142	59	39	11	12.06	25.00	0.001	0.003

MYGH10	348	110	770	205	229	132	16	14.93	25.00	0.001	0.007
NGNH29	465	150	1040	110	81	38	16	10.05	25.00	0.001	0.003
NIGH07	528	200	1600	106	29	10	11	10.05	25.00	0.001	0.003
NIGH12	553	240	780	110	29	9	11	12.65	25.00	0.001	0.003
TCGH16	213	80	680	112	112	334	35	11.27	25.00	0.001	0.007

[1] V_{s30}: time averaged shear-wave velocity in the top 30 m of the soil profile

[2] V_{s0}: shear-wave at the ground surface

[3] $V_{s,depth}$: shear-wave velocity at the depth of the borehole sensor

[4] f_1: the lower frequency limit to estimate individual κ_r

[5] f_2: the upper frequency limit to estimate individual κ_r

[6] $I_{\gamma,0,l}$: the shear-strain index threshold to separate linear and transitional datasets

[7] $I_{\gamma,0,t}$: the shear-strain index threshold to separate transitional and nonlinear datasets

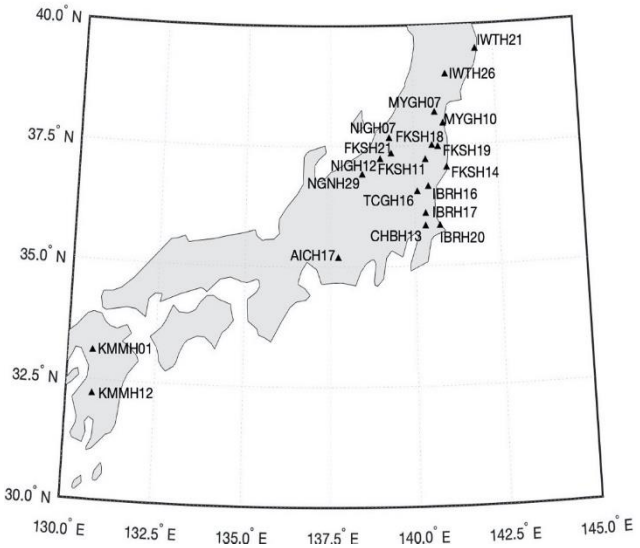

Figure 2. Locations of selected Japanese recording stations in this study.

5. Method

5.1. Identification of the onset of nonlinearity

Identifying ground motions that trigger soil nonlinear behavior is key to evaluate κ estimates beyond the linear-elastic regime empirically. The shear-strain index (I_γ = PGV/V_s), which represents the in-situ deformation, and PGA, which describes the peak amplitude of the ground motion, are commonly used to differentiate linear from nonlinear ground motions. Moreover, the correlation between PGA and I_γ has been shown to be an effective proxy to capture in-situ stress-strain relationships. This correlation has been characterized via the classic hyperbolic model, which fits empirical observations (Chandra et al. 2014, Chandra et al. 2015, Guéguen et al. 2018).

However, there is lack of consensus regarding the sufficiency and efficiency of existing proxies associated with the onset of nonlinear behavior.

We develop appropriate criteria to identify nonlinear ground motions based on examining site response as characterized by both, PGA and I_γ. In this paper, the shear-strain index ($I_{\gamma,0}$) at the surface is defined as follows:

$$I_{\gamma,0} = PGV_{rotD50} / V_{s,0} \tag{6}$$

where $V_{s,0}$ is the shear-wave velocity at the ground surface, and PGV_{rotD50} is the median PGV for all rotated surface ground motions following the approach of Boore (2010). The use of PGV_{rotD50} rather than the PGV from recorded ground motion horizontal components can minimize directionality effects. By applying the classic hyperbolic model to describe the correlation between PGA_{rotD50} and $I_{\gamma,0}$, we find that there is no unique threshold to identify nonlinear ground motions across all study sites. Figure 3 provides examples of theoretical hyperbolic fitting curves at four stations (i.e., IBRH16, IBRH17, IBRH20 and IWTH21) with varying V_{s30} values (from 244 to 626 m/s) to demonstrate the limitations associated with using a single parameter to identify nonlinear ground motions at multiple sites. The scatter points are empirical PGA_{rotD50} and $I_{\gamma,0}$ pairs from recorded ground motions at the sites of interest, while the lines are the fitting curves from the hyperbolic model. It can be observed that the same deformation at various sites would be triggered by different levels of ground shaking (e.g., $I_{\gamma,0}$ of 0.05% will be caused by a PGA_{rotD50} around 100 gals at a NEHRP D site, such as IBRH20 with V_{s30} of 244 m/s, and by a PGA_{rotD50} of 200 gals at a NEHRP C site, such as IBRH16 with V_{s30} of 626 m/s). Meanwhile, if nonlinearity is assumed to be triggered when PGA_{rotD50} is larger than a predetermined threshold, different levels of $I_{\gamma,0}$ will be associated with the onset of soil nonlinearity. Hence, in this work, we propose a hybrid method (further described in the next section) based on both the intensity of the excitation and in-situ deformation to classify ground motions.

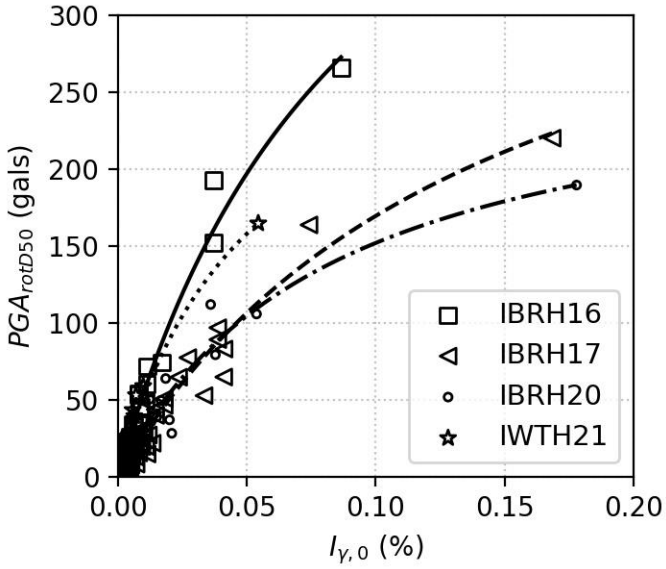

Figure 3. Hyperbolic models fitted to observed PGA_{rotD50} and $I_{\gamma,0}$ data at four study sites.

5.2. Linear, transitional, and nonlinear datasets

Surface and borehole ground motions are considered separately herein, with borehole records assumed to remain in the linear-elastic regime (i.e., they do not trigger nonlinear behavior at depth). Surface records are separated into three sub-datasets, namely linear, transitional (i.e., soil's behavior is between the linear-elastic and nonlinear regimes), and nonlinear ground motions. First, we define a threshold based on $I_{\gamma,0}$ to differentiate linear from transitional records, which is hereafter referred to as $I_{\gamma,0,l}$. Likewise, a transitional threshold, $I_{\gamma,0,t}$, is defined to separate transitional and nonlinear ground motions. The linear $I_{\gamma,0,l}$ threshold is identified as the onset of soil nonlinearity by visual inspections of the corresponding PGA_{rotD50} versus $I_{\gamma,0}$ curve, and corresponds to the point where PGA_{rotD50} values begin to increase at a higher rate with increasing $I_{\gamma,0}$. The transitional $I_{\gamma,0,t}$ threshold captures when the soil nonlinearity becomes more apparent, which corresponds to the point where the second change in slope of the PGA_{rotD50} versus $I_{\gamma,0}$ curve takes place. Figure 4 provides an example of the selection of $I_{\gamma,0,t}$ and $I_{\gamma,0,l}$ at station MYGH10. The threshold separating the linear and transitional ground motions is $I_{\gamma,0,l}$ = 0.001%, while the threshold separating transitional and nonlinear ground motions is $I_{\gamma,0,t}$ = 0.007%.

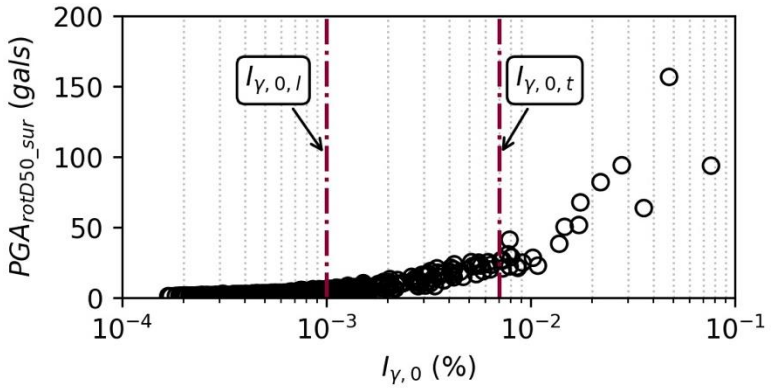

Figure 4. Surface PGA_{rotD50} against $I_{\gamma,0}$ at MYGH10. The red dot-dash lines present the linear and transitional thresholds of $I_{\gamma,0}$.

A maximum PGA_{rotD50} of 25 gals, which is the value adopted by Régnier et al. (2016) to define low-intensity records, is chosen as an additional constraint to avoid linear ground motions being erroneously included into the nonlinear dataset. Thus, linear, transitional, and nonlinear datasets are defined as follows:

- Linear ground motions: records with $I_{\gamma,0}$ less than the $I_{\gamma,0,l}$ threshold.
- Nonlinear ground motions: records with (a) $I_{\gamma,0}$ larger than the $I_{\gamma,0,t}$ threshold and (b) PGA_{rotD50} larger than 25 gals.
- Transitional ground motions: records not classified as either linear or nonlinear.

The validity of the proposed linear, transitional, and nonlinear datasets is then tested by examining the behavior of the shear modulus, G against $I_{\gamma,0}$ at the study sites. The reduction of G for empirical ground motions is estimated as follows (after Guéguen et al., 2019):

$$G/G_{\max} = \frac{PGA_{rotD50}}{PGV_{rotD50}/V_{s,0}} \Bigg/ \left(\frac{PGA_{rotD50}}{PGV_{rotD50}/V_{s,0}} \right)_{\max} \quad (7)$$

The term $\left(\frac{PGA_{rotD50}}{PGV_{rotD50}/V_{s,0}} \right)_{\max}$ is computed from the corresponding average ratio of records with $I_{\gamma,0}$ less than 0.001%, which is the predetermined threshold of $I_{\gamma,0,l}$ for the linear-elastic deformation limit in this work. Figure 5 shows the G/G_{max} versus $I_{\gamma,0}$ curves at all study sites. Identified linear ground motions mainly have G/G_{max} values around 1 (G/G_{max} values higher than 1 result from using mean G values as a proxy for G_{max}), while the ratios corresponding to the nonlinear dataset are generally less than 1 due to the onset of soil nonlinearity. Notably, values of G/G_{max} associated with the transitional dataset are between the linear and nonlinear datasets. It is not clear whether the site response associated with records identified as transitional could be equivalent to a linear-elastic or a nonlinear response (i.e., associated G/G_{max} values vary within a single station and across stations). Hence, the characterization as transitional is deemed appropriate.

5.3. κ_{r_AS} estimates

We use the acceleration spectrum approach (Anderson and Hough, 1984) to estimate κ_{r_AS}. To minimize the variability introduced by the selection of the S-wave window, the entire time series is used. Additionally, compatibility with engineering analysis such as geotechnical site response analysis and ground motion models is desired, and such applications use complete time series. Notably, the differences of κ_{r_AS} values measured from S-wave window and the entire time series are not significant in most cases (Ji et al. 2020).

The variability in estimates of κ_{r_AS} is a function of the selection of the frequency band (Edwards et al. 2015, Perron et al. 2017) among other factors (Ji et al. 2020, Ktenidou et al. 2013). Moreover, soil nonlinearity affects low and high frequencies differently. The onset of nonlinear soil behavior can influence high frequencies first (Bonilla et al. 2011) because larger shear strains are induced in softer, thinner layers located at shallower depths (i.e., in a profile with increasing stiffness with depth). Hence, we compute κ_{r_AS} based on a pre-determined fixed frequency window ($[f_1, f_2]$). The pre-determined f_1 corresponds to the maximum value between 1.4 f_c (where f_c is the earthquake source corner frequency of each record) and 1.4 f_0 (where f_0 is the site's predominant frequency). If f_1 is lower than f_0, the value of κ_{r_AS} will be biased by the site amplification in the high-frequency range (Parolai and Bindi 2004). On the other hand, the f_c requirement is added to reduce the effects of the earthquake source. The value of f_2 is set to be 25 Hz due to consideration of KiK-net instrument's response (Aoi et al., 2004, Fujiwara et al. 2004, Oth et al. 2011, Laurendeau et al. 2013). The arithmetic average of the resulting κ_{r_AS} estimated from two orthogonal horizontal components is used (Ji et al. 2020), and negative κ_{r_AS} values are excluded. These limits ensure a broad frequency bandwidth for κ calculations of at least 10 Hz per record. Additionally, the fixed frequency band reduces potential bias from local amplification effects (Parolai and Bindi, 2004), and minimizes the variability associated with frequency window selections. However, it does not guarantee the most appropriate linear regression for the high-frequency spectral decay, which is the original definition of κ_r by Anderson and Hough (1984). Thus, we further investigate the effects of the frequency band selection for weak and strong ground motion records by comparing the

individual κ_{r_AS} values estimated from a pre-determined fixed frequency window with their counterparts, $\kappa_{r,auto}$, resulting from an automated algorithm which does account for the most appropriate linear regression.

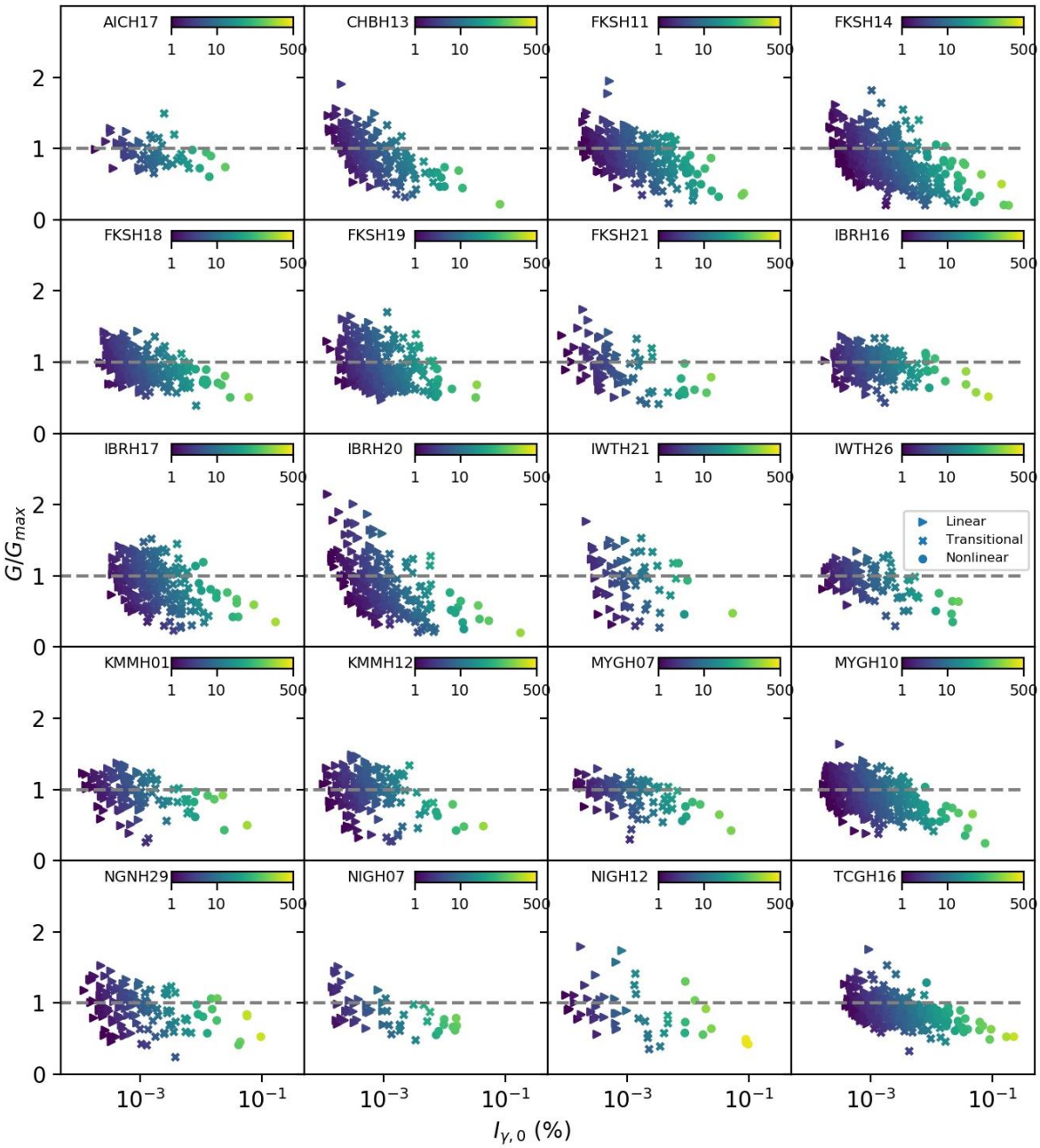

Figure 5. G/G_{max} versus $I_{\gamma,0}$ at study sites. The G_{max} is computed from the average values of $\left(\frac{PGA_{rotD50}}{PGV_{rotD50}/V_{s,0}}\right)$ of records with $I_{\gamma,0}$ less than 0.001%. The colors represent PGA_{rotD50} values.

The automated procedure used in this paper follows a similar protocol as those presented in Sonnemann, and Halldorsson (2017) and Pilz et al. (2019), which focus on finding the optimal frequency band ([f_1, f_2]) to describe the linear decay in the high frequency range. As part of the automated protocol, the minimum f_1 is selected as the maximum value between 1.5f_0, and 1.5fc. To ensure a minimum frequency bandwidth of 10 Hz, the maximum value of f_1 is 15 Hz and the minimum f_2 corresponds to (f_1 +10) Hz. With 0.5 Hz increments in f_1 and f_2, f_1 is varied from the maximum value between 1.5f_0 and 1.5f_c to 15 Hz, while f_2 changes from (f_1+10) Hz to 25 Hz. Going through all the possible combinations of f_1 and f_2, the frequency range with the minimum root mean square error is set as the optimal frequency band. The errors are computed with the following equation after Pilz et al. (2019):

$$P = RMS \Big/ \sqrt{\Delta f} \tag{8}$$

Where Δf is the frequency bandwidth, and RMS is the root mean square error between the fitting line and smoothed FAS. The FAS is smoothed with the Konno-Ohmachi filter with a coefficient of 40 (Konno and Ohmachi, 1998). Finally, a visual inspection for the resulting κ_{r_AS} against epicentral distance plots is conducted to ensure that the $\kappa_{r,auto}$ values follow the expected linear trend.

Figure 6 compares κ_{r_AS} and $\kappa_{r,\ auto}$ for all selected ground motions at FKSH14. Overall, similar κ_{r_AS} and $\kappa_{r,\ auto}$ estimates are observed, but discrepancies are more significant at the ground surface than at depth. The remaining stations also show an acceptable agreement between the two methods at the surface and at depth. Differences between κ_{r_AS} and $\kappa_{r,\ auto}$ are mainly caused by the complexity of some empirical FAS shapes, for example, when multiple linear decaying trends are present in the high-frequency range.

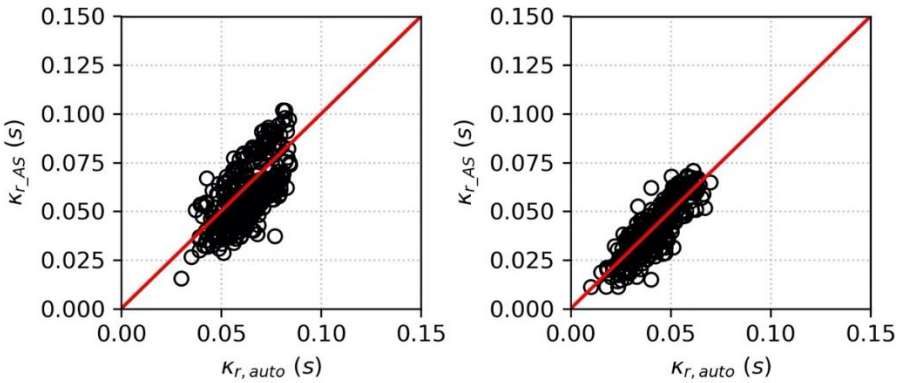

Figure 6. Comparisons of individual κ_r estimates from our automated algorithm, $\kappa_{r,auto}$, and the fixed frequency band method, κ_{r_AS} at FKSH14 for surface (left) and borehole (right).

5.4. κ_0-model

κ_{r_AS} is generally modeled with contributions from a site-specific component (κ_0), a path component (κ_R), and a source component (κ_s). The source component κ_s is often assumed to be negligible and its contribution is reduced by using a dataset with sufficient records (Van Houtte et

al. 2011, Ktenidou et al. 2014). The linear distance-dependency is commonly applied to capture the path component κ_R, which represents source-to-site effects or regional attenuation (Hough et al. 1988, Anderson, 1991, Ktenidou et al. 2013, Boore and Campbell, 2017). Thus, the most commonly accepted model is described below:

$$\kappa_{r\_AS} = \kappa_0 + \kappa_R \times R_e \tag{9}$$

where κ_0 and κ_{r_AS} are in units of time (s), κ_R is in units of second per kilometer (s/km) and R_e refers to epicentral distance in km. This model is valid when a unique source-to-site path is assumed for each record along with a homogeneous and frequency independent seismic quality factor Q (Knopoff 1964).

The model described by Equation (9) is straightforward to apply when only surface linear ground motion datasets are used. However, the incorporation of nonlinear and borehole ground motions adds complexity to the estimation of regional attenuation as captured by κ_R estimates. In this paper, we assume the regional attenuation to be identical for linear and nonlinear ground motions recorded at the ground surface and at depth. Thus, analogous to the formulation suggested by Douglas et al. (2010) for soil and rock sites, we propose a comprehensive model based on Equation (9), which includes linear and nonlinear surface and borehole records:

$$\kappa_{r\_AS} = N_1\kappa_{0\_depth} + N_2\kappa_{0\_lin\_sur} + N_3\kappa_{0\_nl\_sur} + \kappa_R \times R_e \tag{10}$$

where κ_{0_depth} is the site-specific κ_0 at depth, and $\kappa_{0\_lin\_sur}$ and $\kappa_{0\_nl\_sur}$ are the site-specific linear and nonlinear κ_0 at the surface. The coefficients N_1, N_2, N_3, and N_4 are defined as follows:

$$N_1 = \begin{cases} 1 & for\ dataset\ at\ depth \\ 0 & for\ dataset\ at\ the\ surface \end{cases}$$

$$N_2 = \begin{cases} 1 & for\ linear\ dataset\ at\ the\ surface \\ 0 & others \end{cases}$$

$$N_3 = \begin{cases} 1 & for\ nonlinear\ dataset\ at\ the\ surface \\ 0 & others \end{cases}$$

6. Results and Discussion

6.1. Effects of soil nonlinearity on empirical κ_{r_AS}

First, we study the influence of soil nonlinearity on individual κ_{r_AS} estimates at each site. As described in Equation (9), κ_{r_AS} is affected by both local site conditions and path effects in the context of a linear-elastic deformation analysis. To minimize the path component effects as we compare κ_{r_AS} estimates from multiple events with different ground shaking intensities (captured by differences in PGA_{rotD50} and $I_{\gamma,0}$), we separate all records at each site into three groups based on R_e (in km). Bins of R_e considered include [0, 50], [50, 100], and [100, 150]. Within each group,

we assume that the variability from different path contributions is negligible, which allows us to isolate the influence of soil nonlinearity on κ_{r_AS}.

Figure 7 depicts the correlations among κ_{r_AS}, PGA_{rotD50} and $I_{\gamma,0}$ at FKSH14 (V_{s30} = 237 m/s) and MYGH10 (V_{s30} = 348 m/s). It should be noted that we assume that soil nonlinearity is not triggered at depth, and we only study surface records in this section. The triangles, circles, and stars represent the linear, transitional, and nonlinear ground motions, respectively. An overall increasing trend of κ_{r_AS} with increasing intensity of ground shaking (either evidenced by increased PGA or $I_{\gamma,0}$ values) is observed at FKSH14 across the three R_e groups. Similar trends are observed at other seven study sites with V_{s30} less than 400 m/s, which include AICH17, CHBH13, FKSH11, IBRH20, IWTH26, MYGH07, and TCGH16, and at KMMH12 with V_{s30} greater than 400 m/s. The increasing κ_{r_AS} trend with increasing PGA_{rotD50} and $I_{\gamma,0}$ is not as significant at MYGH10 though, which has relatively stiffer site conditions compared to FKSH14. Moreover, either no correlation or a slightly decreasing trend is found at other stiff sites with V_{s30} greater than 400 m/s (i.e., FKSH21, NIGH12, NGNH29, NIGH07, KMMH01, and IBRH16), and at four softer sites with V_{s30} between 300 and 400 m/s (i.e., IWTH21, FKSH18, FKSH19, and IBRH17). We note that the number of available nonlinear records for the R_e ranges at the sites where the decreasing trend is observed is rather limited. Additional nonlinear records at those sites are necessary (i.e., stronger intensity ground motions) to further evaluate the contributing factors to a potential decreasing trend in κ_{r_AS} values. However, in general, we observe that positive correlations between κ_{r_AS} and the intensity of ground shaking are more significant at softer sites (e.g., TCGH16 with V_{s30} of 213 m/s) than at stiffer sites (e.g., KMMH12 with V_{s30} of 408 m/s). The data support that the onset of soil nonlinearity can affect κ_{r_AS} estimates, but such influence is station-dependent. The level of soil nonlinearity can be unique at each specific site (for a similar intensity of ground shaking) because of the complexities of the in situ subsurface conditions. We observe the same patterns in our data when using the automated procedure to compute $\kappa_{r,auto}$.

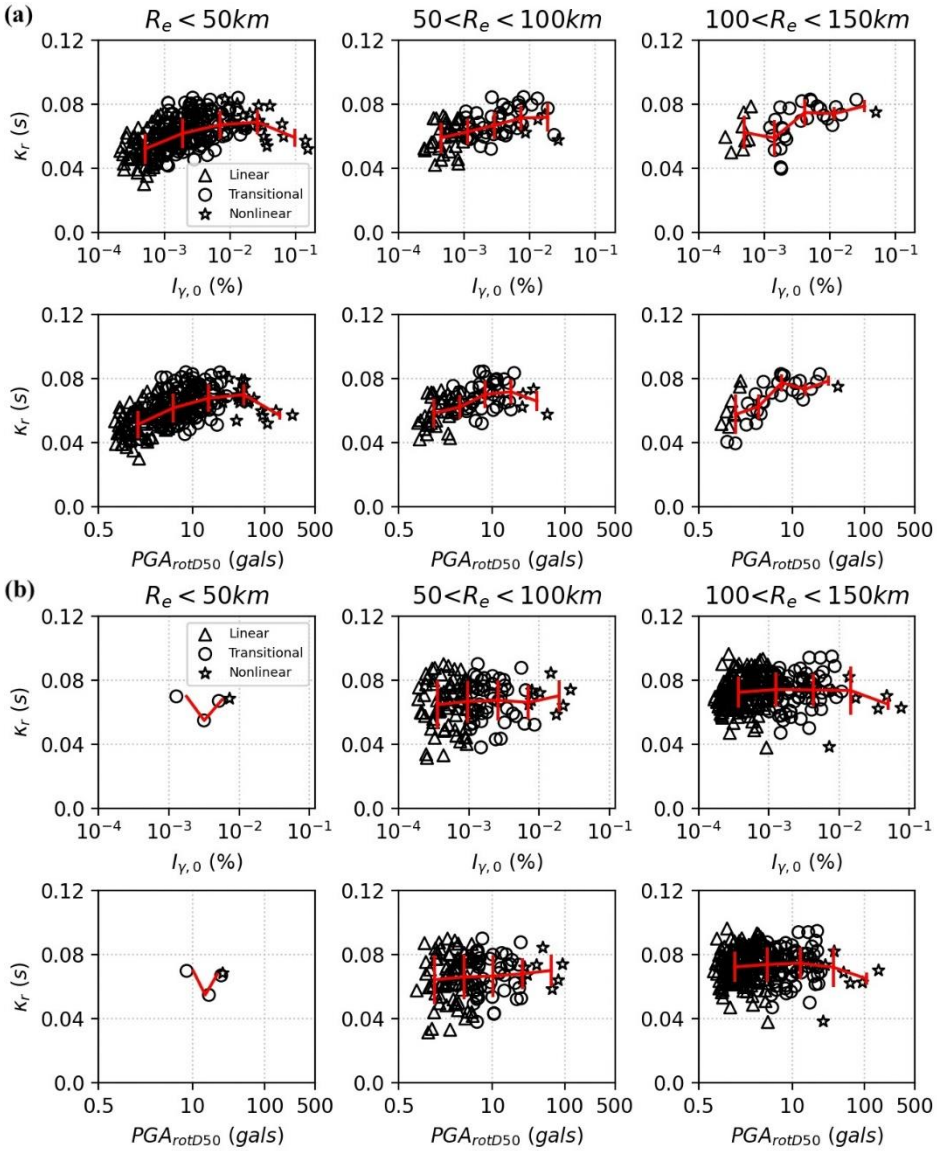

Figure 7. Correlations between surface κ_{r_AS} estimates and ground shaking intensities at (a) FKSH14 (V_{s30} = 237 m/s) and (b) MYGH10 (V_{s30} = 348 m/s). All records are separated into three groups based on the epicentral distance: less than 50 km (left), between 50 and 100 km (middle), and more than 100 km (left). Within each group, records are separated into five bins uniformly, and the vertical red lines are error bars depicting the standard deviation of κ_{r_AS}. The trend line is presented by connecting mean κ_{r_AS} values within each bin.

6.2. Effects of soil nonlinearity on the empirical κ_0-model

Linear, transitional, and nonlinear ground motion datasets are used in this section to allow the assessment of appropriate values of κ_0 beyond the linear-elastic regime. We explore four approaches (i.e., AP1 to AP4) to incorporate records within the transitional dataset into the κ_0-model presented in Equation (5). Table 2 describes how the identified linear, transitional, and nonlinear datasets are used to estimate $\kappa_{0\_lin\_sur}$ and $\kappa_{0\_nl\_sur}$. A modified model is also proposed, where the transitional dataset is analyzed independently:

$$\kappa_{r\_AS} = N_1\kappa_{0\_depth} + N_2\kappa_{0\_lin\_sur} + N_3\kappa_{0\_nl\_sur} + N_4\kappa_{0\_tran\_sur} + \kappa_R \times R_e \quad (11)$$

where

$$N_4 = \begin{cases} 1 & for\ transitional\ dataset\ at\ surface \\ 0 & others \end{cases}$$

And $\kappa_{0\_tran\_sur}$ corresponds to the site-specific κ_0 value resulting from the transitional ground motion dataset. Figures 8 and 9 provide the resulting κ_0 models from each approach at FKSH14 and MYGH10, respectively. Figure 8 shows that κ_{r_AS} and κ_0 values corresponding to the nonlinear ground motions (regardless of the selected approach to construct the nonlinear dataset) are larger than their linear counterparts at FKSH14. However, results at a stiffer station presented in Figure 9 show little disagreement between κ_{r_AS} and κ_0 values corresponding to the linear and nonlinear motions (regardless of the approach to construct each dataset).

Table 2. Ground motion datasets constructed via alternative approaches (AP1 to AP4) explored in this study to implement the κ_0-model.

Approach	$\kappa_{0\_lin\_sur}$	$\kappa_{0\_nl\_sur}$	$\kappa_{0\_tran\_sur}$	κ_{0_depth}	κ_0-model
AP1	Linear dataset	Nonlinear dataset	--	Borehole dataset	Equation (5)
AP2	Linear and transitional datasets	Nonlinear dataset	--	Borehole dataset	Equation (5)
AP3	Linear dataset	Nonlinear and transitional datasets	--	Borehole dataset	Equation (5)
AP4	Linear dataset	Nonlinear dataset	Transitional datasets	Borehole dataset	Equation (6)

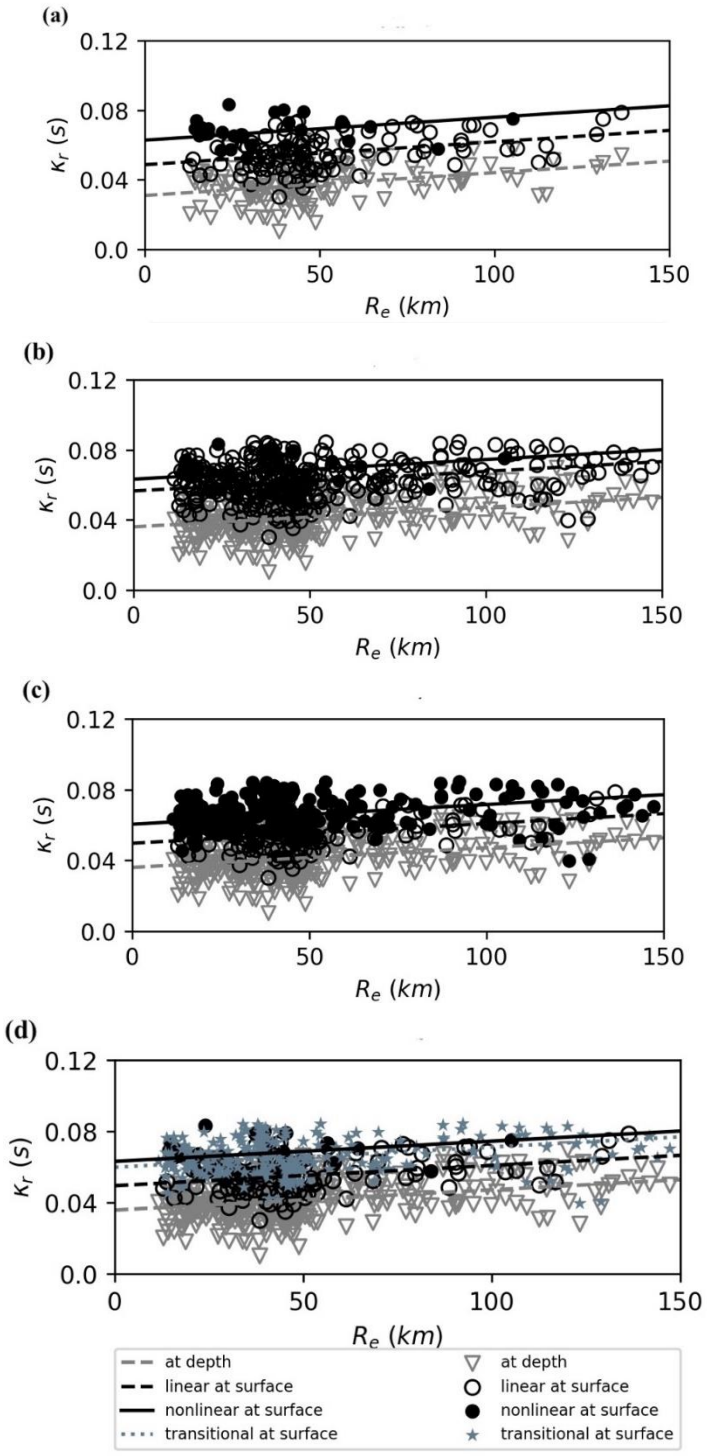

Figure 8. κ_0-model at FKSH14 from datasets defined by (a) AP1, which only considers the linear and nonlinear datasets, (b) AP2, where transitional records are included as part of the linear dataset, (c) AP3, where transitional records are included as part of the nonlinear dataset, and (d) AP4, where the linear, transitional, and nonlinear datasets are considered separately.

Variations in $\kappa_{0\_lin\_sur}$ estimates are observed as a function of the approach considered to construct the linear datasets (see specific values in Table 3). Similarly, variations in $\kappa_{0\_nl\_sur}$ values are also found across the different approaches to define the nonlinear datasets. At FKSH14 (Figure 8), $\kappa_{0\_lin\_sur}$ estimates are more variable as a function of the dataset definitions (with a maximum difference of 16.16% across approaches AP1 to AP4), compared to $\kappa_{0\_nl\_sur}$ values (with a maximum difference of 4.62%). In addition, Figure 8(d) shows that data points corresponding to the transitional dataset are more compatible with their counterparts within the nonlinear dataset, which may indicate that at FKSH14, the level of nonlinearity induced by the transitional dataset is closer to that induced by the ground motions in the nonlinear dataset. Other study sites such as AICH17 and IWTH21 also show that $\kappa_{0\_lin\_sur}$ estimates are more sensitive to dataset selections. In contrast, variations of $\kappa_{0\_lin\_sur}$ and $\kappa_{0\_nl\_sur}$ across datasets at MYGH10 (Figure 9) are small, with maximum differences of only 1.21% and 1.98%, respectively. Large differences in $\kappa_{0\_nl\_sur}$ estimates across datasets are observed at eight sites, but the limited number of nonlinear records at some of those sites (e.g., there are only six nonlinear records at IWTH21, which results in a maximum difference of 47.05% for $\kappa_{0\_lin\_sur}$ and 11.17% for $\kappa_{0\_nl\_sur}$) may be a contributing factor. Adding transitional records to either the linear or the nonlinear dataset at such sites can significantly bias the regression model. In general, differences in the κ_0–model as a function of the selected dataset are observed in 45% of our study sites (with differences in $\kappa_{0\_lin\_sur}$ or $\kappa_{0\_nl\_sur}$ values greater than 10%). This is a relevant observation because it demonstrates the importance of selecting appropriate ground motions even for typical κ_0 estimations (i.e., in the linear-elastic regime) at a given site.

Table 3. Site-specific κ_0 values obtained from different dataset definitions at stations FKSH14 and MYGH10.

	Approach	$\kappa_{0\_lin\_sur}$ (s)	$\kappa_{0\_nl\_sur}$ (s)	$\kappa_{0\_tran\_sur}$ (s)
FKSH14	AP1	0.0487	0.0628	--
	AP2	0.0565	0.0633	--
	AP3	0.0497	0.0605	--
	AP4	0.0496	0.0633	0.0600
	Maximum difference	16.16%	4.62%	
MYGH10	AP1	0.0572	0.0569	--
	AP2	0.0573	0.0567	--
	AP3	0.0566	0.0577	--
	AP4	0.0567	0.0565	0.0579
	Maximum difference	1.21%	1.98%	

Our findings suggest that the development of a κ_0-model beyond the linear-elastic regime is a function of the definition of what constitutes linear and nonlinear ground motion datasets. The identification of transitional ground motion datasets in this study allows us to assess which records provide estimates of κ_{r_AS} that are closer to either the linear or the nonlinear behavior at different sites. Differences in behavior triggered by the records within the transitional database may be caused by unique local site conditions (i.e., the level of soil nonlinearity developed at each site) or by limitations of the simplified definition used herein to classify transitional records (i.e., as a

function of PGA and I_γ). Identifying appropriate linear and nonlinear datasets for κ_{r_AS} estimations requires further research to provide consistent models of near-surface attenuation that can more effectively be implemented from small to large shear strains. However, the site-specific response at each site of interest may lead to challenges in determining appropriate dataset classifications based on a simple, generalized criterion.

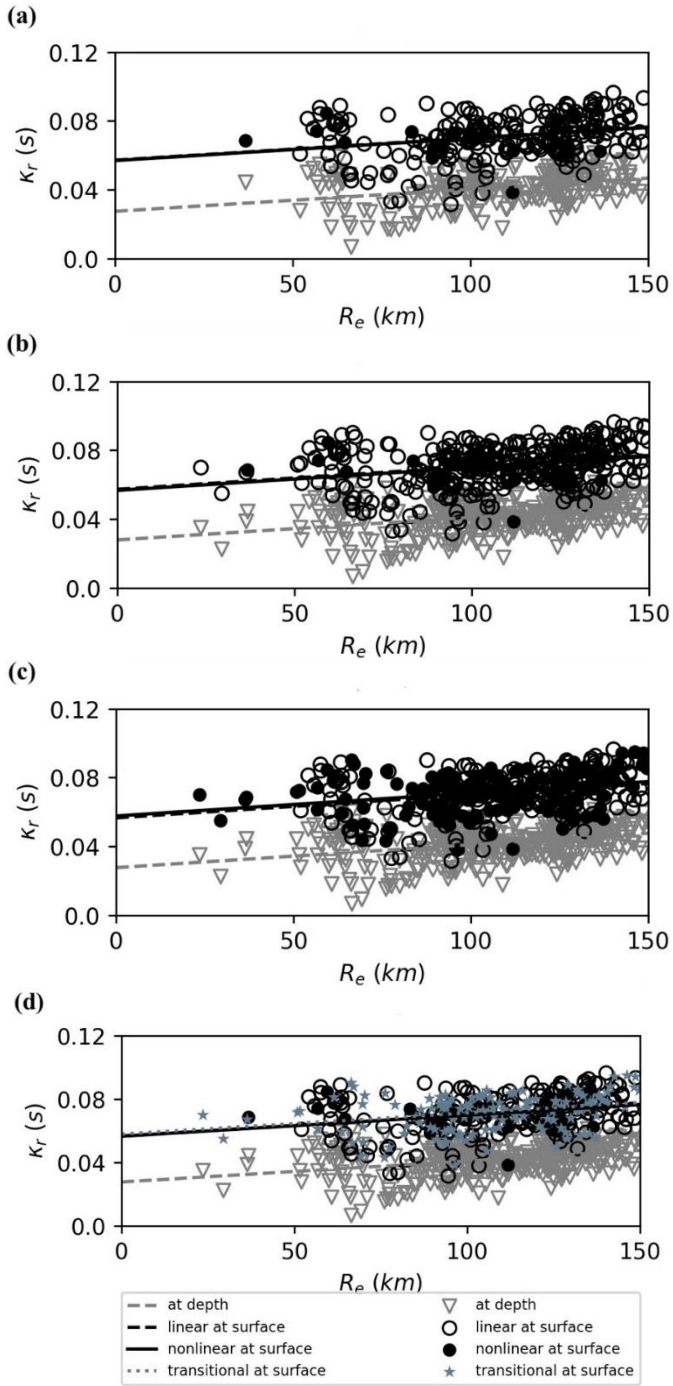

Figure 9. κ_0-model at MYGH10 with datasets defined by (a) AP1, which only considers the linear and nonlinear datasets, (b) AP2, where transitional records are included as part of the

linear dataset, (c) AP3, where transitional records are included as part of the nonlinear dataset, and (d) AP4, where the linear, transitional, and nonlinear datasets are considered separately.

Figure 10 provides ratios of $\kappa_{0\_nl\_sur}/\kappa_{0\_lin\_sur}$ at the 20 study sites based on the four different approaches to construct linear and nonlinear datasets (Table 2) explored in this study. Lager ratios are observed at sites with V_{s30} lower than 300 m/s regardless of the dataset chosen for the κ_0-model. Differences between κ_0 values in the linear and nonlinear regimes seem to be reconciled at sites with higher V_{s30} values, where the ratios fluctuate more closely around unity. When grouping intermediate and strong nonlinear ground motions (i.e., AP3), most stations result in ratios of $\kappa_{0\_nl\_sur}/\kappa_{0\_lin\_sur}$ larger than one (Figure 10c), which can be interpreted as the signature of soil nonlinearity on the near-surface attenuation estimates (i.e., near-surface attenuation increases with larger deformations as the soil nonlinearity is triggered). When treating linear, transitional, and nonlinear datasets independently (i.e., AP4), there are 12 sites with a ratio larger than one. These findings are consistent with the behavior of material damping ratio observed in dynamic laboratory testing of soils. However, potential bias due to the limited number of nonlinear records in our dataset should not be discarded. For instance, we note a few instances when ratios of $\kappa_{0\_nl\_sur}/\kappa_{0\_lin\_sur}$ are lower than one in Figure 10. Those ratios may result from the limited nonlinear records available at those sites coupled with the uncertainties associated with $\kappa_{0\_lin\_sur}$ (e.g., Ji et al., 2020). Overall, the variations observed in the $\kappa_{0\_nl\_sur}/\kappa_{0\_lin\_sur}$ ratio support our hypothesis that soil nonlinearity plays a role on the estimates of near-surface attenuation from recorded ground motions. This effect is station-dependent, and further research is needed to identify the most appropriate parameter or vector of parameters capable of capturing the influence of nonlinear soil behavior on near-surface attenuation. In fact, the weak correlation between V_{s30} and the $\kappa_{0\_nl\_sur}/\kappa_{0\_lin\_sur}$ ratio evidences the challenges in connecting site conditions and soil nonlinearity via a single site parameter. Multiple parameters that can describe attenuation and impedance effects from the shallow and deep geologic structures should be investigated. Finally, the $\kappa_{0\_nl\_sur}/\kappa_{0\_lin\_sur}$ ratio corresponding to IWTH21 (V_{s30} = 521 m/s) is not shown in Figures 10a, c, and d because it is very large (i.e., approximately 1.8). This observation may result from uncertainties associated with κ_{r_AS} values propagating to estimates of κ_0 when the fixed frequency band approach is applied for all records without consideration of the optimal linear decay trend. In fact, the corresponding $\kappa_{0\_nl\_sur}/\kappa_{0\_lin\_sur}$ ratio when implementing the automated procedure is approximately 0.90. Finally, to minimize the potential bias caused by the classification of the transitional dataset as either linear or nonlinear in this study, we adopt the AP4 approach (which considers the linear, transitional, and nonlinear datasets independently) to evaluate predictions of near-surface attenuation in the next section of this paper.

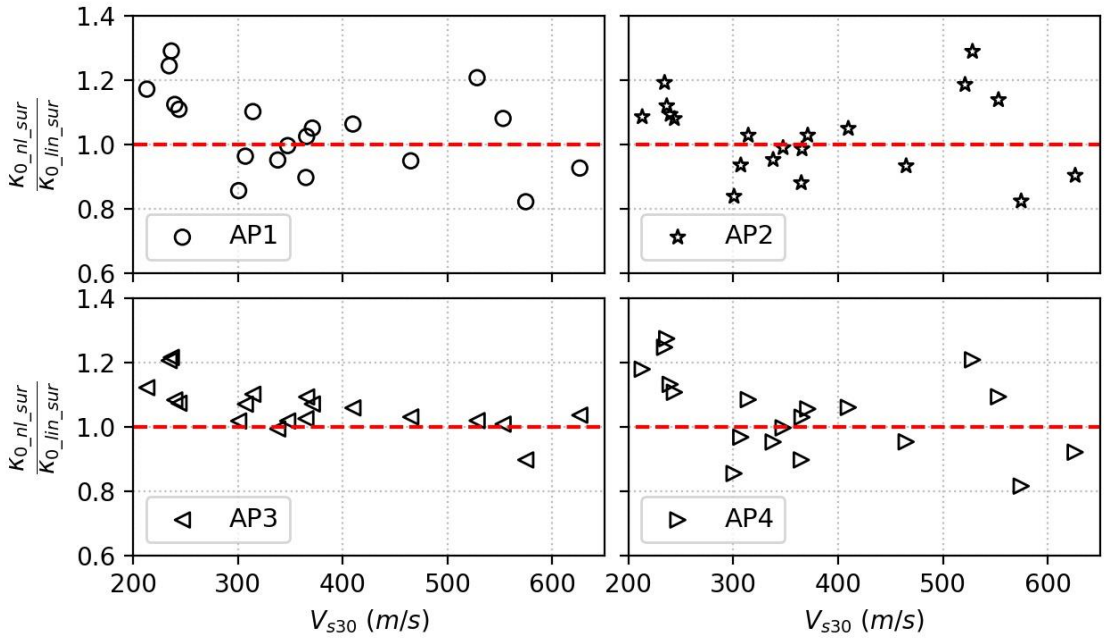

Figure 10. Ratio of $\kappa_{0\_nl\_sur}/\kappa_{0\_lin\_sur}$ at selected sites corresponding to the four approaches to define datasets explored in this study.

6.3. Effects of soil nonlinearity on predicted near-surface attenuation

Site-specific $\kappa_{0\_lin\_sur}$ or $\kappa_{0\_nl\_sur}$ values from Equation (11) allow for the comparison of empirical estimates of near-surface attenuation in the linear and nonlinear regimes. In this section, we investigate the influence of soil nonlinearity on predictions of near-surface attenuation as captured by κ_{0_pred}:

$$\kappa_{0\_pred} = \kappa_{r\_AS\_sur} - R_e \kappa_R \tag{12}$$

where $\kappa_{r\_AS\_sur}$ refers to the individual κ_{r_AS} value for a surface ground motion, and the path-component, κ_R, is based on the values derived with Equation (11) at each site of interest. We assume that by removing the effect of the path-component κ_R from individual $\kappa_{r\_AS\_sur}$ values, the remaining κ_{0_pred} is able to provide an approximation to the attenuation contributed by the shallower sedimentary deposits per event. Thus, we can get an estimate of the near-surface attenuation for each observed ground motion at the site of interest.

Figure 11 provides comparisons between κ_{0_pred} and ground shaking intensity as captured by PGA_{rotD50} and $I_{\gamma,0}$ at FKSH14 and MYGH10. Values of κ_{0_pred} first increase and then decrease with increasing PGA_{rotD50} and $I_{\gamma,0}$ at FKSH14, which are also observed at other six sites (i.e., CHBH13, IBRH20, IWTH26, KMMH12, MYGH07, TCGH16). In contrast, only a weak correlation to the intensity of ground shaking is observed at MYGH10, which further shows that soil nonlinearity effects are not statistically significant at this site for the records selected in this study. Moreover, Figure 12 compares the probability distribution of κ_{0_pred} values from the linear, transitional, and nonlinear datasets at FKSH14 and MYGH10. The resulting κ_{0_pred} values are fitted with a Gaussian distribution and the corresponding probability density functions (PDFs) are represented by red

lines. A shift to the right (i.e., toward larger κ_{0_pred} values) of theoretical PDFs is observed at FKSH14 as ground motions from the linear, transitional, and nonlinear datasets are considered, which are also observed at other four stations (i.e., CHBH13, FKSH11, IBRH20 and TCGH16). The mean κ_{0_pred} estimates change from 0.0496 s for the linear dataset to 0.0633 s for the nonlinear dataset at FKSH14 (i.e., a difference of 27.6%). In contrast, the variation of mean κ_{0_pred} between linear and nonlinear datasets at MYGH10 is 0.9%. Generally, an increase and then decrease trend of κ_{0_pred} estimates from the linear, transitional and nonlinear datasets are observed at eleven sites, and the remaining four sites show a decrease of mean κ_{0_pred} estimates from linear to transitional motions. Overall, we find that Figures 11 and 12 not only support our hypothesis that the effects of soil nonlinearity on κ are station-dependent, but also show an increasing trend in near-surface attenuation with increasing ground shaking intensity.

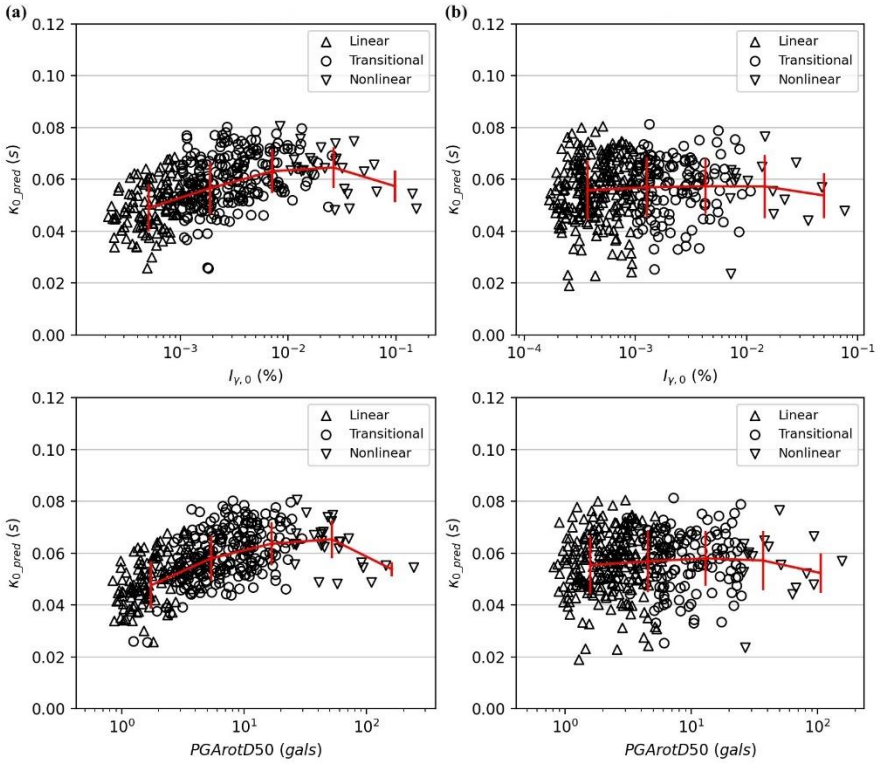

Figure 11. Correlations between surface κ_{0_pred} and ground shaking intensities at (a) FKSH14 (V_{s30} = 237 m/s) and (b) MYGH10 (V_{s30} = 348 m/s). At each site, records are separated into five bins uniformly, and the error bars (vertical red lines) show the standard deviation of κ_{0_pred}. The trend line is presented by connecting mean values of κ_{0_pred} within each bin.

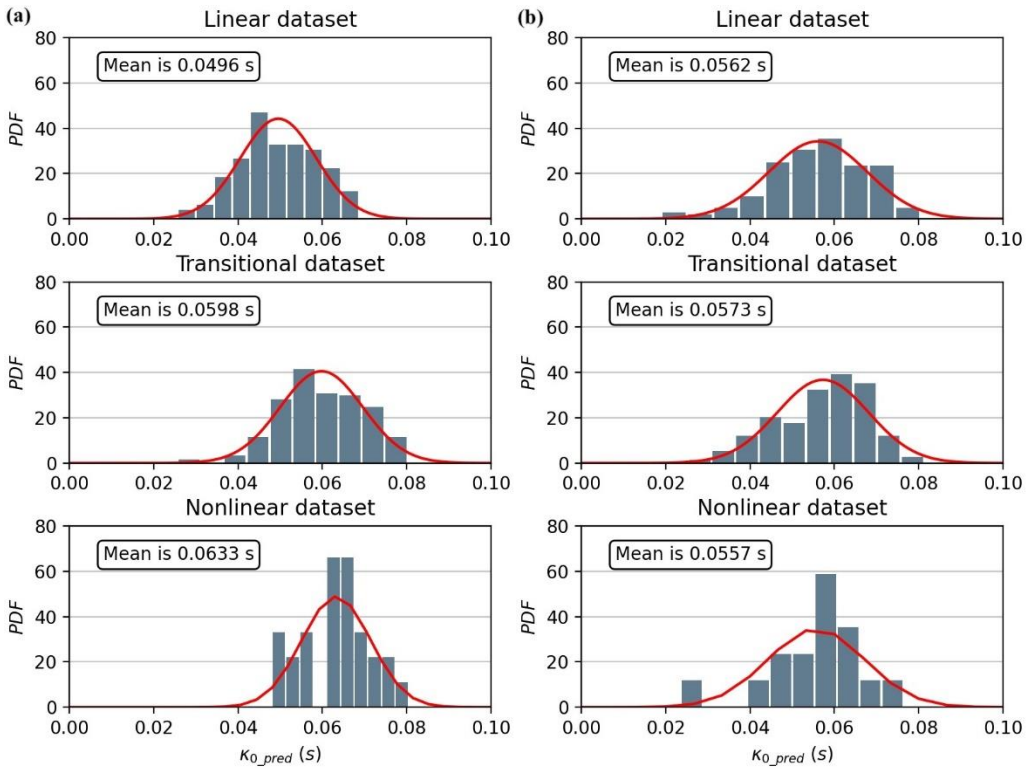

Figure 12. Observed distribution of κ_{0_pred} at (a) FKSH14 (V_{s30} = 237 m/s) and (b) MYGH10 (V_{s30} = 348 m/s). The red lines present the theoretical probability density function (PDF) fitted with a Gaussian distribution.

7. Conclusions

In this work, we investigated the influence of soil nonlinear behavior on individual κ_{r_AS} and site-specific κ_0 estimates at 20 stations selected from the KiK-net database. We also examined the effects of the frequency band selection on κ_{r_AS} estimates by comparing a predetermined fixed-frequency window approach with an automated procedure, capable of finding the optimal frequency band per record for all records at each site. The selection of a common, fixed and broader frequency band for κ_{r_AS} estimations reduced the scatter and bias in the data, while providing reasonable estimations of κ_{r_AS}. Hence, the analyses presented in this paper were conducted with κ_r values estimated by the fixed-frequency band approach.

A consistent identification of ground motions that trigger nonlinear behavior in sedimentary deposits is necessary to quantify near-surface attenuation beyond the linear-elastic regime. Based on the examination of an in-situ stress-strain proxy, namely the correlation between PGArotD50 and $I_{\gamma,0}$, we found that variations of shear strains with ground shaking intensity at the onset of nonlinear soil behavior is site-specific. A unique threshold for a single parameter, whether it is PGArotD50 or $I_{\gamma,0}$, was not able to capture the onset of soil nonlinearity at our study sites consistently across all sites. Hence, we proposed a hybrid method to classify linear and nonlinear ground motions considering both, PGArotD50 and $I_{\gamma,0}$, which resulted in linear, transitional, and nonlinear datasets at each site.

We investigated the influence of soil nonlinearity on κ_{r_AS} estimates by separating the records into different groups based on epicentral distance to reduce path-component effects. An increasing κ_{r_AS} trend with increasing PGArotD50 or $I_{\gamma,0}$ was observed at about half of the study sites. Additionally, we found that κ_0 models can be biased by the definition of linear and nonlinear ground motion datasets. Hence, we proposed a κ_0 model that minimizes this bias by independently incorporating linear, transitional, and nonlinear records in the κ_0 regression. Our results revealed discrepancies between $\kappa_{0\_lin\_sur}$ (corresponding to the linear-elastic regime) and $\kappa_{0\_nl\_sur}$ (from the nonlinear regime) at most sites. Such discrepancies were more prevalent among softer sites, and particularly more significant at sites with V_{s30} less than 300 m/s.

The hypothesis posed and tested in this paper focused on the effects of ground shaking intensity on induced shear strains in sedimentary deposits and associated consequences on the attenuation experienced by seismic waves (particularly in the high frequency range). In general, we find that soil nonlinear behavior can affect estimates of κ_{r_AS} and κ_0, but our results show that this influence is station-dependent. This is reasonable because the wave propagation of short wavelength waves is highly affected by heterogeneities in the soil or rock, local geologic structures, and topography. Further research and strong ground motion data are necessary to identify local site conditions conducive to generate significant changes in near-surface attenuation as captured by κ_0 beyond the linear-elastic regime.

8. Data and Resources

Accelerograms and geotechnical data are downloaded from the KiK-net network at http://www.kyoshin.bosai.go.jp (last accessed May 2020). The earthquake information is available from F-net network at http://www.fnet.bosai.go.jp/top.php (last accessed May 2020).

9. Acknowledgements

The authors would like to appreciate that the National Research Institute for Earth and Disaster Prevention (NIED) provides the ground motion and site information. The authors acknowledge Dr. Adrian Rodriguez-Marek and Mahdi Bahrampouri for sharing their processed dataset. This work was sponsored by the U.S. Geological Survey under Grant Number G19AP00058. The views and conclusions contained in this document are those of the authors and should not be interpreted as representing the opinions or policies of the U.S. Geological Survey.

10. Reference

Anderson, J. G., & Hough, S. E. (1984). A model for the shape of the Fourier amplitude spectrum of acceleration at high frequencies. *Bull Seismol Soc Am*. **74**, no. 5, 1969-1993.

Anderson, J.G. (1991). A preliminary descriptive model for the distance dependence of the spectral decay parameter in southern California. *Bull Seismol Soc Am*. **81**, no. 6, 2186-2193.

Al Atik, L., Kottke, A., Abrahamson, N. and Hollenback, J., (2014). Kappa (κ) scaling of ground-motion prediction equations using an inverse random vibration theory approach. Bulletin of the Seismological Society of America, 104, no. 1, 336-346.

Aoi, S., T. Kunugi, and H. Fujiwara (2004). Strong-motion seismograph network operated by NIED: K-NETand KiK-net, J. Japan Assoc. Earthq.Eng. 4, no. 3, 65–74.

Bahrampouri, M., Rodriguez-Marek, A., Shahi, S., & Dawood, H. (202x). An update database for ground motion parameters for KiK-net records. Submitted to Earthquake Spectra.

Bonilla, L.F., Tsuda, K., Pulido, N., Régnier, J. and Laurendeau, A., 2011. Nonlinear site response evidence of K-NET and KiK-net records from the 2011 off the Pacific coast of Tohoku Earthquake. Earth, planets and space, 63(7), p.50.

Boore, D.M., 2003. Simulation of ground motion using the stochastic method. *Pure and applied geophysics*, 160(3-4), pp.635-676.

Boore, D. M., Watson-Lamprey, J., & Abrahamson, N. A. (2006). Orientation-independent measures of ground motion. Bull Seismol Soc Am. 96, no. 4A, 1502-1511.

Boore, D.M. and Campbell, K.W., 2017. Adjusting central and eastern North America ground-motion intensity measures between sites with different reference-rock site conditions. Bulletin of the Seismological Society of America, 107(1), pp.132-148.

Campbell, K.W., 2003. Prediction of strong ground motion using the hybrid empirical method and its use in the development of ground-motion (attenuation) relations in eastern North America. Bulletin of the Seismological Society of America, 93(3), pp.1012-1033.

Cabas, A., Rodriguez-Marek, A., & Bonilla, L. F. (2017). Estimation of Site-Specific Kappa (κ0)-Consistent Damping Values at KiK-Net Sites to Assess the Discrepancy between Laboratory-Based Damping Models and Observed Attenuation (of Seismic Waves) in the Field. *Bull Seismol Soc Am*. **107**, no. 5, 2258-2271.

Chandra, J., Guéguen, P. and Bonilla, L.F., 2014. Application of PGV/VS proxy to assess nonlinear soil response–from dynamic centrifuge testing to Japanese K-NET and KiK-net data. In Second European Conference on Earthquake Engineering and Seismology, Istanbul Aug (pp. 25-29).

Chandra, J., Guéguen, P., Steidl, J.H. and Bonilla, L.F., 2015. In situ assessment of the G–γ curve for characterizing the nonlinear response of soil: Application to the Garner Valley downhole array and the wildlife liquefaction array. Bulletin of the Seismological Society of America, 105(2A), pp.993-1010.

Chandra, J., Gueguen, P. and Bonilla, L.F., 2016. PGA-PGV/Vs considered as a stress–strain proxy for predicting nonlinear soil response. Soil dynamics and earthquake engineering, 85, pp.146-160.

Darragh, R.B. and Shakal, A.F., 1991. The site response of two rock and soil station pairs to strong and weak ground motion. Bulletin of the Seismological Society of America, 81(5), pp.1885-1899.

Darendeli M. B. (2001). Development of a new family of normalized modulus reduction and material damping curves, Ph.D. Thesis, University of Texas at Austin, Austin, Texas.

Dimitriu, P., Theodulidis, N., Hatzidimitriou, P., & Anastasiadis, A. (2001). Sediment non-linearity and attenuation of seismic waves: a study of accelerograms from Lefkas, western Greece. *Soil Dynam Earthquake Eng*. **21**, no.1, 63-73.

Durward, J.A., Boore, D.M., Joyner, W.B., Durward, J.A., Boore, D.M. and Joyner, W.B., 1996. The amplitude dependence of high-frequency spectral decay: constraint on soil nonlinearity. In Proc, of the International Workshop on Site Response Subjected to Strong Earthquake Motions (pp. 82-103).

Douglas, J., Gehl, P., Bonilla, L.F. and Gélis, C., (2010). A κ model for mainland France. Pure Appl Geophys. 167, no.11, 1303-1315.

Edwards, B., Ktenidou, O.J., Cotton, F., Abrahamson, N., Van Houtte, C. and Fäh, D., (2015). Epistemic uncertainty and limitations of the κ 0 model for near-surface attenuation at hard rock sites. *Geophys J Int.* **202**, no. 3, 1627-1645.

Fujiwara, H., S. Aoi, T. Kunugi, and S. Adachi (2004). Strong-motion observation networks of NIED: K-NETand KiK-net, National Research Institute for Earth Science and Disaster Prevention.Garcia, D., Wald, D. J., & Hearne, M. G. (2012). A global earthquake discrimination scheme to optimize ground-motion prediction equation selection. Bull Seismol Soc Am. 102, no.1, 185-203.

Guéguen, P., Bonilla, L.F. and Douglas, J., 2019. Comparison of Soil Nonlinearity (In Situ Stress–Strain Relation and G/Gmax Reduction) Observed in Strong-Motion Databases and Modeled in Ground-Motion Prediction EquationsComparison of Soil Nonlinearity Observed in Strong-Motion Databases and Modeled in GMPEs. Bulletin of the Seismological Society of America, 109(1), pp.178-186.

Hough, S.E., Anderson, J.G., Brune, J., Vernon III, F., Berger, J., Fletcher, J., Haar, L., Hanks, L. and Baker, L., 1988. Attenuation near Anza, California. Bulletin of the Seismological Society of America, 78(2), pp.672-691.

Idriss, I.M., Dobry, R.U. and Sing, R.D., 1978. Nonlinear behavior of soft clays during cyclic loading. *Journal of geotechnical and geoenvironmental engineering*, 104.

Ji, C., Cabas, A., Cotton, F., Pilz, M. and Bindi, D., 2020. Within-Station Variability in Kappa: Evidence of Directionality Effects. Bull Seismol Soc Am., 110(3), pp.1247-1259.

Knopoff, L. (1964). Q, Rev. Geophys. 2, no. 4, 625–660.

Ktenidou, O. J., Gélis, C., & Bonilla, L. F. (2013). A study on the variability of kappa (κ) in a borehole: Implications of the computation process. *Bull Seismol Soc Am*. **103**, no.2A, 1048-1068.

Ktenidou, O. J., Cotton, F., Abrahamson, N. A., & Anderson, J. G. (2014). Taxonomy of κ: A review of definitions and estimation approaches targeted to applications. *Seismol Res Lett*. **85**, no.1, 135-146.

Ktenidou, O.J., Abrahamson, N.A., Drouet, S. and Cotton, F., (2015). Understanding the physics of kappa (κ): Insights from a downhole array. Geophys J Int. 203, no. 1, 678-691.

Konno, K. and Ohmachi, T., 1998. Ground-motion characteristics estimated from spectral ratio between horizontal and vertical components of microtremor. Bulletin of the Seismological Society of America, 88(1), pp.228-241.

Laurendeau, A., Cotton, F., Ktenidou, O. J., Bonilla, L. F., & Hollender, F. (2013). Rock and stiff-soil site amplification: Dependency on VS 30 and kappa (κ 0). Bull Seismol Soc Am. 103, no. 6, 3131-3148.

Lacave-Lachet, C., Bard, P.Y., Gariel, J.C. and Irikura, K., 2000. Straightforward methods to detect non-linear response of the soil. Application to the recordings of the Kobe earthquake (Japan, 1995). Journal of seismology, 4(2), pp.161-173.

Nakano, K., Matsushima, S., & Kawase, H. (2015). Statistical properties of strong ground motions from the generalized spectral inversion of data observed by K-NET, KiK-net, and the JMA Shindokei network in Japan. *Bull Seismol Soc Am*.**105**, no. 5, 2662-2680.

Oth, A., Parolai, S. and Bindi, D., (2011). Spectral analysis of K-NET and KiK-net data in Japan, Part I: Database compilation and peculiarities. Bull Seismol Soc Am. 101, no.2, 652-666.

Parolai, S. and Bindi, D., (2004). Influence of soil-layer properties on k evaluation. Bulletin of the Seismological Society of America, 94(1), pp.349-356.

Pilz, M., Cotton, F., Zaccarelli, R. and Bindi, D., (2019). Capturing Regional Variations of Hard-Rock Attenuation in Europe. *Bull Seismol Soc Am*.

Perron, V., Hollender, F., Bard, P. Y., Gélis, C., Guyonnet-Benaize, C., Hernandez, B., & Ktenidou, O. J. (2017). Robustness of kappa (κ) measurement in low-to-moderate seismicity areas: Insight from a site-specific study in Provence, France. Bull Seismol Soc Am. 107, no.5, 2272-2292.

Régnier, J., Cadet, H., Bonilla, L.F., Bertrand, E. and Semblat, J.F., 2013. Assessing nonlinear behavior of soils in seismic site response: Statistical analysis on KiK-net strong-motion data. Bulletin of the Seismological Society of America, 103(3), pp.1750-1770.

Régnier, J., Cadet, H. and Bard, P.Y., 2016. Empirical Quantification of the Impact of Nonlinear Soil Behavior on Site ResponseEmpirical Quantification of the Impact of Nonlinear Soil Behavior on Site Response. Bulletin of the Seismological Society of America, 106(4), pp.1710-1719.

Rong, M., Wang, Z., Woolery, E.W., Lyu, Y., Li, X. and Li, S., 2016. Nonlinear site response from the strong ground-motion recordings in western China. Soil Dynamics and Earthquake Engineering, 82, pp.99-110.

Seed, H.B., Wong, R.T., Idriss, I.M. and Tokimatsu, K., 1986. Moduli and damping factors for dynamic analyses of cohesionless soils. *Journal of geotechnical engineering*, 112(11), pp.1016-1032.

Sonnemann, T. and Halldorsson, B., 2017, June. Towards an Automated Kappa Measurement Procedure. In International Conference on Earthquake Engineering and Structural Dynamics (pp. 39-52). Springer, Cham.

Trifunac, M.D. and Todorovska, M.I., 1996. Nonlinear soil response—1994 Northridge, California, earthquake. Journal of geotechnical engineering, 122(9), pp.725-735.

Van Houtte, C., Drouet, S., & Cotton, F. (2011). Analysis of the origins of κ (kappa) to compute hard rock to rock adjustment factors for GMPEs. *Bull Seismol Soc Am*.**101**, no. 6, 2926-2941.

Van Houtte, C., Ktenidou, O.J., Larkin, T. and Holden, C., (2014). Hard-site κ 0 (kappa) calculations for Christchurch, New Zealand, and comparison with local ground-motion prediction models. Bull Seismol Soc Am.104, no. 4, 1899-1913.

Yu, G., Anderson, J.G. and Siddharthan, R.A.J., 1993. On the characteristics of nonlinear soil response. Bulletin of the Seismological Society of America, 83(1), pp.218-244.

Zalachoris, G. and Rathje, E.M., 2015. Evaluation of one-dimensional site response techniques using borehole arrays. Journal of Geotechnical and Geoenvironmental Engineering, 141(12), p.04015053.

Part III: Estimations of κ_0 in Low-to-moderate Seismicity Regions

1. Introduction

In recent years, the interest in the site-specific high-frequency spectral decay parameter, κ_0, has increased, not only because of its proven advantages when adjusting ground motion prediction models (GMPEs) from host to target regions, and its applications in site-specific PSHA. Values of κ_0 can also be used to constrain high frequencies for synthetic or simulated ground motions (e.g., Boore 2003, Cabas et al., 2015; Cabas and Rodriguez-Marek 2017). Additional applications include the use of κ for development of site-specific amplification factors for Ground Motion Response Spectra screening at facilities with limited site characterization data (e.g., EPRI 2013). It has also been shown that the seismic motion on rock and stiff-soil sites does not only depend on the shear wave velocity of near-surface materials, but also on κ_0 (Laurendeau et al., 2013).

Uncertainty in the estimation of κ is large (Ktenidou et al., 2014), and may have important implications for seismic risk in practice; especially at rock sites, where the estimation of the attenuation or damping in the profile is vital to assessing appropriate levels of high-frequency (> ~5 Hz) design motions. Site attenuation controls the scaling from soft to hard rock at high frequencies (Cotton et al., 2006), as it governs ground motion characteristics in the high-frequency range at short site-source distances, where crustal damping effects are small (Hashash et al., 2014). This is especially relevant for low-attenuating hard rock sites, where the high-frequency components of the ground motion can be underestimated (Perron et al., 2017). Consequently, adjusting the GMPEs to hard-rock conditions is sensitive to κ_0 (Ktenidou et al., 2016). For instance, the Pegasos Refinement Project (Biro and Renault 2012) demonstrated how κ_0 corrections from soft-rock to hard-rock conditions can lead to differences up to a factor of 3 in the high-frequency part of the response spectrum (Ktenidou et al., 2016).

The objective of this study is to provide recommendations to address the scarcity of records in low-to-moderate seismicity regions and the difficulty in defining their site-specific attenuation models. These efforts will lead naturally into developing more consistent host-to-target adjustments used in site-specific PSHA. Shear wave velocity profiles are more "readily available and well-understood" at local scales, however site-specific κ_0 values continue to impose challenges within the PSHA framework. Finally, the convolution of bedrock hazard curves with the site response at the site of interest also requires a consistent treatment of attenuation to avoid double-counting of epistemic uncertainty in the κ_0 scaling factors (Ktenidou et al., 2016).

2. Current approaches to estimate κ_0 for low-to-moderate seismicity regions

Different methodologies to compute κ values or estimate them based on other site parameters such as $V_{s,30}$ have populated the literature recently (e.g., Silva and Darragh, 1995; Chandler et al. 2006; Drouet et al., 2010; Van Houtte et al., 2011). However, the scatter in κ_0-$V_{s,30}$ relationships is rather large. When it comes to site-specific PSHA, one of the main challenges is the lack of data (particularly events with magnitudes larger than 3), and usable bandwidth (Perron et al., 2017) in low-to-moderate seismicity regions (i.e., target regions), which does not allow the use of the

acceleration spectrum methodology (i.e., Anderson and Hough, 1984 approach, shown in Figure 4b) to compute individual values of κ. The latter is often used for the host regions, which are not usually affected by paucity of records. Consequently, it is critical to understand the differences among the resulting κ_0 values from each method before using them in different engineering seismology and earthquake engineering applications, especially in the context site-specific seismic hazard analysis in low-to-moderate seismicity regions. For example, estimates of κ_0 for Central and Eastern US (CEUS) have been based on a comprehensive literature review (Hashash et al., 2014) as shown in Figure 1, where an average value of 6±2 ms was selected as representative for the region. Campbell et al., (2013) provides more details on the determination of such value.

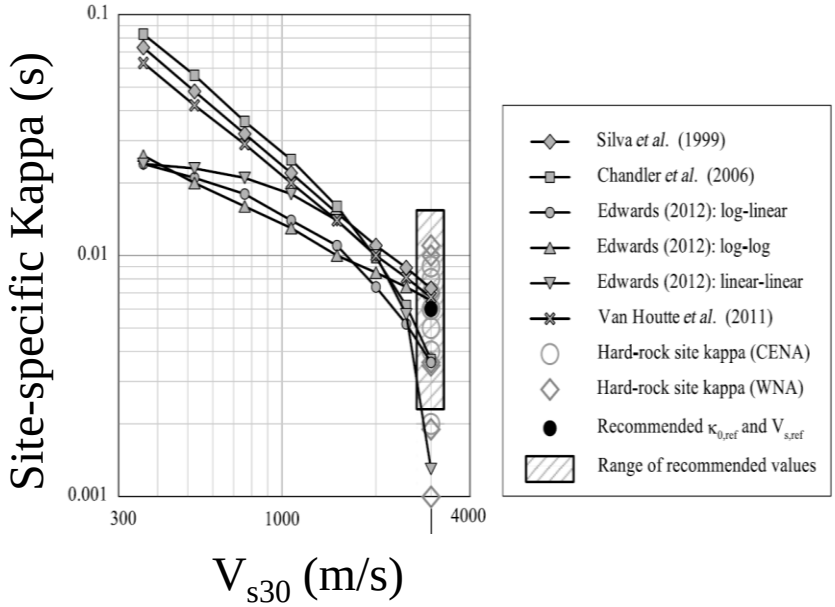

Figure 1. Estimates of hard-rock κ_0 values for CEUS (modified after Hashash et al., 2014)

Ktenidou et al., (2016) explored four approaches (two band-limited and two broadband) for estimating the site κ_0 for rock sites in the NGA-East database: the acceleration slope (AS) above the corner frequency, the displacement slope (DS) below the corner frequency, the broadband (BB) fit of the spectrum, and the response spectral shape (RESP) template. These authors found discrepancies among the various methods, and only the broadband methods provided a good agreement with the value provided in the literature for the region (i.e., 6±2 ms). More recent efforts also include the DS, and AS methods to estimate κ_0 in mainland France (i.e., Perron et al., 2017). However, all the approaches considered still require the availability of ground motion records.

2.1. Displacement Spectrum Method (Biasi and Smith, 2001)

This is a promising method as it was derived for low-magnitude events and, as indicated by Perron et al., (2017) because "the flatness of the displacement source spectrum below the corner frequency is better understood than the ω^{-2} fall-off above the corner frequency" (i.e., the assumption used in the AS method). The method is based on estimating κ from the low-frequency portion of small earthquake displacement spectra. It was introduced by Biasi and Smith (2001), where data from approximately 263 earthquakes with a median magnitude of ML=0.3 were evaluated. One of the

largest sources of uncertainties of this method is the estimation of corner frequencies for the selected events, as they are a function of moment magnitude and stress drop. The latter may not be well constrained for low-to-moderate seismicity regions (Ktenidou et al., 2016).

2.2. Transfer Function Method (Drouet et al., 2010)

Drouet et al. (2010) measured a site-specific (independent of distance) κ_0 value directly on the high frequency portion (i.e., frequencies higher than 10 Hz) of a site's transfer function (TF). Source-path-site inversions using weak to moderate earthquakes recorded by the French Accelerometric Network were used to estimate the TF at 76 stations. Kappa values derived from this methodology are called κ_{0_TF} (Ktenidou et al., 2013). This method quantifies the attenuation of seismic waves taking place between a reference rock horizon and the ground surface. The difference between κ_{0_AS} (or κ_{r_AS}) calculated for bedrock conditions and its counterpart obtained at the ground surface, known as $\Delta\kappa_{0\_AS}$ (Cabas and Rodriguez-Marek, 2017) has also been proposed as a metric to capture the contribution of sedimentary deposits to overall path attenuation. Thus, κ_{0_TF} estimates should be theoretically equivalent to $\Delta\kappa_{0\_AS}$.

2.3. Inverse Random Vibration Theory Method (Al Atik et al., 2014)

This method allows the computation of κ-scaling factors for GMPEs so that high-frequency spectral content can be more robustly characterized. The method is based on inverse random vibration theory as implemented in the computer program Strata (Kottke and Rathje, 2008a,b). A Fourier amplitude spectrum (FAS) is derived such that it is consistent with the response spectrum from the selected GMPE (Al Atik et al., 2014). Then, estimated FAS is scaled from in accordance with the assumed κ values for host and target regions. Finally, Random vibration theory (Cartwright and Longuet-Higgins, 1956) is used to convert the κ-adjusted FAS to response spectrum. This method also provides κ-scaling factors computed as the ratio of the κ-scaled response spectra to the GMPE response spectra (Al ATik et al., 2014).

Previous studies have compared κ_0 from Anderson and Hough (1984) with the displacement method (e.g., Ktenidou et al 2016, and Perron et al 2017). The κ_{DS} estimates are believed to better represent material damping in the shallower layers, while the κ_{AS} estimates may reflect a net effect of damping and amplification (Ktenidou et al., 2016). Most recent studies have found κ values from the DS to be larger than the ones obtained from the AS method.

3. Comparison between $\Delta\kappa_{0\_AS}$ and κ_{0_TF}

3.1. Study Sites

We evaluate four recording stations from the KiK-Net database with an empirical site response that can be represented by a one–dimensional (1D) theoretical linear elastic analysis. Stations FKSH14 and IBRH10 were classified as sites with low inter–event variability and a good fit to 1D theoretical formulations of wave propagation (LG) by Thompson et al. (2012), which make them suitable for linear elastic site response validation analysis. Sites OSKH01 and SZOH25 were not included in the Thompson et al. (2012) study. However, after comparing 1D linear–elastic theoretical and empirical transfer functions at these two sites, they were also deemed suitable for

linear elastic site response validation analysis. While the intent of this research is not to assess the appropriateness of 1D site response models, it is important to select study sites with compatible theoretical and empirical transfer functions. The aforementioned agreement will allow the investigation of the sources of uncertainty in κ_{0_TF} values to remain independent from the chosen site response model. The V_s profiles of our study sites are shown in Figure 2.

Site OSKH01 is a single layer site. Site SZOH25 is a multiple–layer site with a smooth V_s gradient. At FKSH14, there is an impedance contrast (calculated as the ratio between the product of density and V_s of the overlying layer and the product of the density and V_s of the underlying layer; hence, the lower the ratio, the stronger the impedance contrast) of 0.24 at 52m depth. At IBRH10, the V_s gradient is slightly higher than for SZOH25 and the impedance contrast at bedrock is significant (i.e., 0.31). Values of V_{s30}, V_{s_mean} (time–averaged V_s for entire depth of soil profile), depth to bedrock and NEHRP (National Earthquake Hazards Reduction Program) site classification (FEMA 450) for each site are provided in Table 1.

Table 1. Selected Site Details and Classification

Site Name	Depth to Bedrock (m)	V_{s30} (m/s)	V_{s_mean} (m/s)	NEHRP Site Classification
OSKH01	550	500	500	C
SZOH25	328	347.3	589.1	D
FKSH14	106	251.3	654	D
IBRH10	518	200	531.3	D

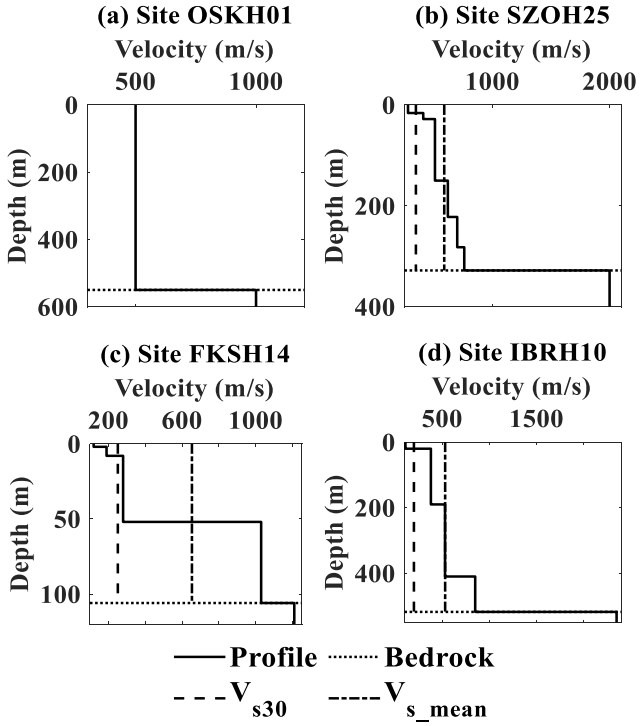

Figure 2. Shear wave velocity profiles of selected KiK–net sites.

3.2. Ground Motion Selection

We compute κ_{0_TF} for at least 10 ground motion pairs at each site. We use both horizontal components of the recorded motions and values of κ_{0_TF} are reported as the average per horizontal component orientation. Each selected record is processed following protocols in Dawood et al. (2016) to comply with signal processing recommendations, such as baseline corrections and adequate noise windows (Ktenidou et al., 2012). The initial selection criteria of processed ground motions is based on peak ground accelerations lower than 10cm/s^2 (to avoid the onset of soil nonlinear behavior), moment magnitudes between 3 and 5, epicentral distances less than 180 km (to avoid bias by multiple seismic ray paths) and shear strain index, I_γ (defined as the ratio of peak ground velocity and V_{s30}; Chandra et al., 2016) less than 0.1% (to further constrain only linear motions) as shown in Table 2.

The values of $\kappa_{r\_AS\_bedrock}$, $\kappa_{r\_AS\_surface}$, and κ_{0_TF} are evaluated between 10Hz and 25Hz. For further screening, we identify amplification peaks on the empirical transfer functions taking place beyond 8Hz, so that $\kappa_{r\_AS\_bedrock}$, $\kappa_{r\_AS\_surface}$, and κ_{0_TF} are calculated for attenuating slopes not biased by high–frequency amplifications (Parolai and Bindi, 2004). Transfer functions are calculated using smoothed FAS of each horizontal component by applying the Konno–Ohmachi filter (Konno & Ohmachi, 1998). Any recording affected by site amplification peaks beyond 8Hz is rejected from our database (Parolai and Bindi, 2004).

Table 2. Initial Ground Motion Screening Criteria

Parameter	Value	Reference
SNR	<3	Ktenidou et al. (2012)
PGA	<10cm/s^2	Ktenidou et al. (2012)
Magnitude	3-5	Drouet et al. (2010)
Epicentral Distance	<180km	Anderson and Hough (1984)
Shear Strain Index	<0.1%	Cabas et al. (2017)

3.3. Empirical estimations of $\Delta\kappa_{0\_AS}$ and κ_{0_TF}

At every site, we estimate site–specific kappa from recorded motions. Since the FAS method is more commonly used, we calculate and compare values of $\Delta\kappa_{0\_AS}$ and κ_{0_TF} using the recorded motions at bedrock and at the ground surface. For each recorded motion pair at the study sites, $\kappa_{r\_AS\_bedrock}$ is evaluated from the spectral decay of acceleration FAS evaluated from the recording observed at the bedrock. $\kappa_{r\_AS\_surface}$ is calculated from the spectral decay of acceleration FAS of the recording at the surface. Thus, the site–specific kappa estimate, $\Delta\kappa_{0\_AS}$, is obtained as follows:

$$\Delta\kappa_{0\_AS} = \kappa_{r\_AS\_surface} - \kappa_{r\_AS\_bedrock} \quad \textbf{(1)}$$

Empirical transfer functions (ETF) are calculated as the ratio of the FAS corresponding to the surface ground motion and the FAS corresponding to the ground motion recorded at the downhole sensor depth for each recording pair at the study sites. As proposed by Drouet et al. (2010), κ_{0_TF} is then calculated as the slope of the decaying peaks in the high-frequency range of

the ETF. We hypothesize that the contribution of the sedimentary deposit to the overall attenuation can be captured by κ_{0_TF} analogously to the characterization provided by $\Delta\kappa_{0\_AS}$ (Cabas and Rodriguez-Marek, 2017). Importantly, the same frequency range (i.e., f_1 and f_2) is used to evaluate κ_{0_TF} from the ETF and the acceleration method for each record.

Tables 3 to 6 provide our resulting empirical site-specific values of κ at each study site. Estimates of κ_{0_TF} and $\Delta\kappa_{0\_AS}$ are provided per horizontal component and also as the mean of both horizontal components of selected ground motions. Selected frequency bands per record are also provided and remain the same for both the acceleration and the transfer function method. As a result, we find a very good agreement among estimates of site-specific κ values for all study sites. Such observation is very promising, as we further explore the transfer function method as a viable approach to obtain estimates of site-specific κ values in low-to-moderate seismicity regions. Ongoing research by the PI includes the assessment of theoretical TFs from one-dimensional site response models as proxies for ETFs to estimate κ_{0_TF}.

4. Conclusions

The estimation of site–specific kappa from the acceleration spectrum method (κ_{0_AS}) is needed for various engineering design purposes and requires the availability of abundant ground motion data. At low–to–moderate seismicity regions such as Central and Eastern United States, the scarcity of strong ground motion data limits the applicability of κ_{0_AS}.

In this study, we first examined the equivalency between empirical estimates of $\Delta\kappa_{0\_AS}$ and κ_{0_TF}. Based on four sites and a total of 50 records, our study found that the estimates of both $\Delta\kappa_{0\_AS}$ and κ_{0_TF} agree if kappa values at bedrock ($\kappa_{r\_AS\_bedrock}$), at the ground surface ($\kappa_{r\_AS\_surface}$) and the ones from the empirical transfer function at the site of interest (κ_{0_TF}) are evaluated within the same frequency bands.

Future research will investigate site-specific κ_{0_TF} from theoretical transfer functions from site response analysis and κ_{0_IRVT} values resulting from inverse random vibration theory (Al Atik et al. 2014), their limitations and similarities to the near-surface attenuation as captured by the κ_0 values from the traditional acceleration method (Anderson and Hough 1984).

Table 3: Ground Motion Details and Empirical Site-Specific Kappa (in sec) at OSKH01 (single-layer site)

Record Number	Magnitude (Mw)	Epicentral Distance (km)	PGA (g) (NS)	PGA (g) (EW)	NS Direction						EW Direction					
					f_1 (Hz)	f_2 (Hz)	Acceleration Spectrum Method ($\Delta\kappa_{0\_AS\_NS} = \kappa_{r\_AS\_Sur\_NS} - \kappa_{r\_AS\_Bore\_NS}$)			Transfer Function Method	f_1 (Hz)	f_2 (Hz)	Acceleration Spectrum Method ($\Delta\kappa_{0\_AS\_EW} = \kappa_{r\_AS\_Sur\_EW} - \kappa_{r\_AS\_Bore\_EW}$)			Transfer Function Method
							$\kappa_{r\_AS\_Bore\_NS}$	$\kappa_{r\_AS\_Sur\_NS}$	$\Delta\kappa_{0\_AS\_NS}$	$\kappa_{0\_TF\_NS}$			$\kappa_{r\_AS\_Bore\_EW}$	$\kappa_{r\_AS\_Sur\_EW}$	$\Delta\kappa_{0\_AS\_EW}$	$\kappa_{0\_TF\_EW}$
45990	3.9	34.5	0.007	0.007	12.5	22.5	0.0023	0.0327	0.0304	0.0304	15.0	25.0	0.0100	0.0230	0.0130	0.0130
45999	4.0	86.0	0.002	0.003	13.5	25.0	0.0178	0.0583	0.0405	0.0405	15.0	25.0	0.0118	0.0172	0.0054	0.0054
46002	4.3	66.1	0.006	0.010	14.0	24.0	0.0576	0.0743	0.0166	0.0166	14.0	24.0	0.0435	0.0303	-0.0132	-0.0132
46007	4.5	62.4	0.004	0.005	15.0	25.0	0.0153	0.0443	0.0290	0.0290	14.5	25.0	0.0049	0.0180	0.0131	0.0131
62332	3.9	83.8	0.002	0.002	15.0	25.0	0.0348	0.0638	0.0290	0.0290	14.0	25.0	0.0281	0.0321	0.0039	0.0039
62342	4.3	92.1	0.003	0.004	15.0	25.0	0.0455	0.0604	0.0149	0.0149	15.0	25.0	0.0337	0.0265	-0.0071	-0.0071
62345	4.3	84.0	0.002	0.002	14.5	24.5	0.0418	0.0773	0.0356	0.0356	14.0	24.5	0.0289	0.0327	0.0037	0.0037
90554	4.2	56.1	0.002	0.002	10.0	20.0	0.0161	0.0483	0.0322	0.0322	14.5	24.5	0.0368	0.0518	0.0150	0.0150
93053	4.8	58.3	0.005	0.005	10.0	25.0	0.0269	0.0526	0.0257	0.0257	15.0	25.0	0.0221	0.0308	0.0087	0.0087
130642	4.8	98.8	0.006	0.005	10.5	21.5	0.0261	0.0316	0.0055	0.0055	15.0	25.0	0.0241	0.0403	0.0162	0.0162
					$\Delta\kappa_{0\_NS\_Emp\_Mean}$				**0.0260**	**0.0260**	**$\Delta\kappa_{0\_EW\_Emp\_Mean}$**				**0.0059**	**0.0059**
					Standard Deviation				**0.0100**	**0.0100**	**Standard Deviation**				**0.0092**	**0.0092**

Table 4: Ground Motion Details and Empirical Site-Specific Kappa (in sec) at SZOH25 (multi-layer, smooth Vs gradient site, deep impedance contrast)

Record Number	Magnitude (M_w)	Epicentral Distance (km)	PGA (g) (NS)	PGA (g) (EW)	NS Direction						EW Direction					
					f_1 (Hz)	f_2 (Hz)	Acceleration Spectrum Method ($\Delta\kappa_{0\_AS\_NS} = \kappa_{r\_AS\_Sur\_NS} - \kappa_{r\_AS\_Bore\_NS}$)			Transfer Function Method	f_1 (Hz)	f_2 (Hz)	Acceleration Spectrum Method ($\Delta\kappa_{0\_AS\_EW} = \kappa_{r\_AS\_Sur\_EW} - \kappa_{r\_AS\_Bore\_EW}$)			Transfer Function Method
							$\kappa_{r\_AS\_Bore\_NS}$	$\kappa_{r\_AS\_Sur\_NS}$	$\Delta\kappa_{0\_AS\_NS}$	$\kappa_{0\_TF\_NS}$			$\kappa_{r\_AS\_Bore\_EW}$	$\kappa_{r\_AS\_Sur\_EW}$	$\Delta\kappa_{0\_AS\_EW}$	$\kappa_{0\_TF\_EW}$
49372	3.6	73.7	0.0003	0.0003	13.0	23.0	-0.0019	0.0525	0.0544	0.0544	10.0	21.5	0.0497	0.0447	-0.0050	-0.0050
49382	4.4	94.5	0.0003	0.0005	13.5	23.5	-0.0096	0.0572	0.0668	0.0668	15.0	25.0	0.0362	0.0704	0.0342	0.0342
49384	3.9	80.8	0.0003	0.0003	14.5	24.5	0.0143	0.0854	0.0711	0.0711	10.5	21.5	0.0376	0.0442	0.0066	0.0066
49387	4.1	69.6	0.0008	0.0008	10.0	20.0	0.0415	0.0521	0.0106	0.0106	15.0	25.0	0.0339	0.0923	0.0584	0.0584
49399	3.6	39.3	0.0005	0.0005	11.5	23.0	-0.0076	0.0586	0.0662	0.0662	14.5	24.5	0.0458	0.0677	0.0219	0.0219
49411	4.0	50.9	0.0004	0.0003	10.0	20.0	0.0442	0.0612	0.0170	0.0170	11.5	22.5	0.0539	0.0524	-0.0015	-0.0015
73026	4.3	136.6	0.0003	0.0004	11.0	22.5	0.0108	0.0554	0.0446	0.0446	15.0	25.0	0.0494	0.0747	0.0253	0.0253
81921	4.1	15.4	0.0011	0.0009	14.5	24.5	0.0095	0.0876	0.0782	0.0782	10.5	20.5	0.0345	0.0385	0.0040	0.0040
87619	3.9	32.7	0.0007	0.0006	11.0	22.0	-0.0066	0.0252	0.0318	0.0318	10.5	20.5	-0.0214	0.0030	0.0244	0.0244
165233	4.4	174.3	0.0004	0.0004	14.5	24.5	0.0259	0.0650	0.0391	0.0391	15.0	25.0	0.0229	0.0507	0.0278	0.0278
					$\Delta\kappa_{0\_NS\_Emp\_Mean}$				**0.0480**	**0.0480**	**$\Delta\kappa_{0\_EW\_Emp\_Mean}$**				**0.0196**	**0.0196**
					Standard Deviation				**0.0221**	**0.0221**	**Standard Deviation**				**0.0182**	**0.0182**

Table 5: Ground Motion Details and Empirical Site-Specific Kappa (in sec) at FKSH14 (multi-layer, shallow impedance contrast site)

Record Number	Magnitude (M_w)	Epicentral Distance (km)	PGA (g) (NS)	PGA (g) (EW)	NS Direction						EW Direction					
					f_1 (Hz)	f_2 (Hz)	Acceleration Spectrum Method ($\Delta\kappa_{0\_AS\_NS} = \kappa_{r\_AS\_Sur\_NS} - \kappa_{r\_AS\_Bore\_NS}$)			Transfer Function Method	f_1 (Hz)	f_2 (Hz)	Acceleration Spectrum Method ($\Delta\kappa_{0\_AS\_EW} = \kappa_{r\_AS\_Sur\_EW} - \kappa_{r\_AS\_Bore\_EW}$)			Transfer Function Method
							$\kappa_{r\_AS\_Bore\_NS}$	$\kappa_{r\_AS\_Sur\_NS}$	$\Delta\kappa_{0\_AS\_NS}$	$\kappa_{0\_TF\_NS}$			$\kappa_{r\_AS\_Bore\_EW}$	$\kappa_{r\_AS\_Sur\_EW}$	$\Delta\kappa_{0\_AS\_EW}$	$\kappa_{0\_TF\_EW}$
9673	4.8	111.3	0.002	0.003	11.5	21.5	0.0477	0.0561	0.0083	0.0083	10.5	20.5	0.0590	0.0785	0.0195	0.0195
64601	4.2	132.0	0.003	0.002	11.0	21.0	0.0477	0.0785	0.0308	0.0308	10.0	20.0	0.0599	0.0941	0.0342	0.0342
89057	4.3	87.1	0.001	0.001	12.5	22.5	0.0367	0.0991	0.0624	0.0624	15.0	25.0	0.0485	0.0355	-0.0130	-0.0130
108184	3.9	16.2	0.006	0.005	13.0	23.0	0.0071	0.0535	0.0464	0.0464	11.5	24.5	0.0180	0.0532	0.0352	0.0352
108226	3.9	19.9	0.007	0.007	15.0	25.0	0.0323	0.0767	0.0444	0.0444	10.0	20.0	0.0649	0.0904	0.0255	0.0255
108229	4.2	31.8	0.002	0.002	10.0	20.0	0.0442	0.0538	0.0096	0.0096	10.0	20.0	0.0412	0.0709	0.0297	0.0297
108235	4.2	25.6	0.002	0.003	12.5	22.5	0.0286	0.0633	0.0347	0.0347	14.0	25.0	0.0282	0.0329	0.0047	0.0047
108256	4.4	62.7	0.003	0.004	12.0	25.0	0.0377	0.0565	0.0188	0.0188	14.5	24.5	0.0411	0.0382	-0.0029	-0.0029
108288	3.9	26.8	0.005	0.004	10.0	21.5	0.0387	0.0414	0.0027	0.0027	15.0	25.0	0.0337	0.0296	-0.0041	-0.0041
117542	4.3	34.2	0.005	0.005	11.0	22.0	0.0322	0.0542	0.0220	0.0220	15.0	25.0	0.0131	0.0178	0.0047	0.0047
117551	3.8	17.8	0.006	0.007	12.5	24.5	0.0137	0.0651	0.0514	0.0514	10.0	21.5	0.0422	0.0659	0.0237	0.0237
117552	4.3	46.8	0.003	0.004	10.0	22.0	0.0422	0.0585	0.0163	0.0163	15.0	25.0	0.0336	0.0288	-0.0048	-0.0048
121976	3.9	52.4	0.002	0.002	10.0	25.0	0.0303	0.0489	0.0186	0.0186	10.0	20.0	0.0376	0.0694	0.0318	0.0318
122006	3.8	112.6	0.001	0.002	12.5	25.0	0.0244	0.0509	0.0265	0.0265	15.0	25.0	0.0307	0.0376	0.0069	0.0069
127503	3.9	55.0	0.001	0.001	12.0	23.5	0.0311	0.0578	0.0267	0.0267	10.0	20.0	0.0298	0.0702	0.0404	0.0404
					$\Delta\kappa_{0\_NS\_Emp\_Mean}$				**0.0280**	**0.0280**	**$\Delta\kappa_{0\_EW\_Emp\_Mean}$**				**0.0154**	**0.0154**
					Standard Deviation				**0.0165**	**0.0165**	**Standard Deviation**				**0.0169**	**0.0169**

Table 6: Ground Motion Details and Empirical Site-Specific Kappa (in sec) at IBRH10 (multi-layer, higher Vs gradient, deep impedance contrast)

Record Number	Magnitude (M_w)	Epicentral Distance (km)	PGA (g) (NS)	PGA (g) (EW)	NS Direction						EW Direction					
					f_1 (Hz)	f_2 (Hz)	Acceleration Spectrum Method ($\Delta\kappa_{0\_AS\_NS} = \kappa_{r\_AS\_Sur\_NS} - \kappa_{r\_AS\_Bore\_NS}$)			Transfer Function Method	f_1 (Hz)	f_2 (Hz)	Acceleration Spectrum Method ($\Delta\kappa_{0\_AS\_EW} = \kappa_{r\_AS\_Sur\_EW} - \kappa_{r\_AS\_Bore\_EW}$)			Transfer Function Method
							$\kappa_{r\_AS\_Bore\_NS}$	$\kappa_{r\_AS\_Sur\_NS}$	$\Delta\kappa_{0\_AS\_NS}$	$\kappa_{0\_TF\_NS}$			$\kappa_{r\_AS\_Bore\_EW}$	$\kappa_{r\_AS\_Sur\_EW}$	$\Delta\kappa_{0\_AS\_EW}$	$\kappa_{0\_TF\_EW}$
109418	4.2	144.6	0.001	0.001	11.0	21.0	-0.0403	0.0366	0.0769	0.0769	10.5	20.5	-0.0274	0.0457	0.0731	0.0731
109476	4.0	132.1	0.002	0.003	11.0	21.0	-0.0122	0.0666	0.0789	0.0789	10.5	20.5	0.0047	0.0755	0.0707	0.0707
117946	3.9	122.0	0.004	0.006	11.0	21.0	-0.0068	0.0592	0.0661	0.0661	10.5	20.5	0.0086	0.0761	0.0675	0.0675
117948	4.3	97.3	0.003	0.003	11.5	21.5	-0.0070	0.0572	0.0641	0.0641	10.5	20.5	0.0174	0.0846	0.0672	0.0672
122538	4.6	152.6	0.001	0.001	11.0	21.5	-0.0046	0.0701	0.0747	0.0747	10.5	20.5	0.0229	0.0822	0.0592	0.0592
122550	4.2	98.3	0.003	0.003	11.0	21.0	0.0093	0.0675	0.0581	0.0581	10.5	20.5	0.0047	0.0761	0.0715	0.0715
122552	3.9	94.9	0.003	0.003	11.5	21.5	0.0092	0.0736	0.0644	0.0644	11.0	21.0	0.0307	0.1048	0.0741	0.0741
122567	4.0	145.3	0.001	0.001	10.5	20.5	-0.0264	0.0343	0.0607	0.0607	10.5	20.5	-0.0304	0.0594	0.0898	0.0898
122581	4.2	96.5	0.003	0.003	10.5	20.5	-0.0053	0.0392	0.0445	0.0445	10.5	20.5	-0.0153	0.0627	0.0780	0.0780
128032	4.2	97.5	0.004	0.003	10.5	20.5	-0.0317	0.0317	0.0633	0.0633	10.5	20.5	-0.0057	0.0663	0.0720	0.0720
128033	3.8	113.3	0.003	0.002	12.0	22.0	-0.0018	0.0516	0.0534	0.0534	10.5	20.5	-0.0066	0.0759	0.0825	0.0825
128041	4.0	132.6	0.001	0.001	11.0	21.0	-0.0041	0.0515	0.0556	0.0556	10.5	20.5	-0.0090	0.0608	0.0698	0.0698
128042	3.9	104.5	0.002	0.002	11.0	21.5	-0.0184	0.0370	0.0554	0.0554	10.5	20.5	-0.0351	0.0473	0.0824	0.0824
					$\Delta\kappa_{0\_NS\_Emp\_Mean}$				**0.0628**	**0.0628**	**$\Delta\kappa_{0\_EW\_Emp\_Mean}$**				**0.0737**	**0.0737**
					Standard Deviation				**0.0095**	**0.0095**	**Standard Deviation**				**0.0076**	**0.0076**

5. Data and Resources

Accelerograms and geotechnical data are downloaded from the KiK-net network at http://www.kyoshin.bosai.go.jp (last accessed August 2020).

6. Acknowledgements

The authors would like to appreciate that the National Research Institute for Earth and Disaster Prevention (NIED) provides the ground motion and site information. This work was sponsored by the U.S. Geological Survey under Grant Number G19AP00058. The views and conclusions contained in this document are those of the authors and should not be interpreted as representing the opinions or policies of the U.S. Geological Survey.

7. References

Al Atik, L., Kottke, A., Abrahamson, N., Hollenback, J., (2014) "Kappa (κ) Scaling of Ground-Motion Prediction Equations Using an Inverse Random Vibration Theory Approach," *Bulletin of the Seismological Society of America,* Vol. 104, pp. 336–346, February 2014, DOI: 10.1785/0120120200.

Anderson, J.G., (1991) "A preliminary descriptive model for the distance dependence of the spectral decay parameter in southern California," *Bulletin of the Seismological Society of America,* Vol. 81, pp. 2186–2193.

Anderson, J.G., Hough, S.E., (1984) "A Model for the Shape of the Fourier Amplitude Spectrum of Acceleration at High-Frequencies," *Bulletin of the Seismological Society of America,* Vol. 74, No. 5, pp. 1969–1993.

Aoi, S., Kunugi, T., Fujiwara, H., (2004) "Strong-motion seismograph network operated by NIED: K-NET and KiK-net," *Journal of Japan Association for Earthquake Engineering,* Vol. 4, pp. 65–74.

Biasi, G., Smith, K.D., Final Project Report, (2001) "Site effects for seismic monitoring stations in the vicinity of Yucca Mountain, Nevada," Prepared for the US DOE/UCCSN Cooperative Agreement Number DE-FC08-98NV12081, Task 12, Southern Great Basin Seismic Network Operations (SGBSN), MOL.20011204.0045.

Biro, Y., P. Renault, P., (2012) "Importance and impact of host-to-target conversions for ground motion prediction equations in PSHA," *In: Proceedings of the 15th World Conference on Earthquake Engineering,* 1855, Lisbon, Portugal.

Boore, D.M., (2003) "Simulation of Ground Motion Using the Stochastic Method," *Pure Applied Geophysics,* Vol 160, pp. 635-676.

Boore, D.M., (2016) "Determining Generic Velocity and Density Models for Crustal Amplification Calculations, with an Update of the Boore and Joyner (1997) Generic Site Amplification for VS(Z) 760 m/s," *Bulletin of the Seismological Society of America,* Vol. 106, No. 1, pp. 316–320, February 2016, doi: 10.1785/0120150229.

Boore, D., Joyner, W., (1997) "Site amplifications for generic rock sites," *Bulletin of the Seismological Society of America,* Vol. 87, No. 2, pp. 327–341.

Cabas, A., Rodriguez-Marek, A., (2017) "Vs-κ0 Correction Factors for Input Ground Motions Used in Seismic Site Response Analyses," *Earthquake Spectra,* Volume 33, No. 3, Pages 917–941, August 2017, doi: 10.1193/22315EQS188M.

Cabas, A., Rodriguez-Marek, A., Bonilla, L.F., (2017) "Estimation of Site-Specific Kappa (κ0)-Consistent Damping Values at KiK-Net Sites to Assess the Discrepancy between Laboratory-Based Damping Models and Observed Attenuation (of Seismic Waves) in the Field," *Bulletin of the Seismological Society of America,* Vol. 107, No. 5, pp. 2258–2271, October 2017, doi: 10.1785/0120160370.

Cartwright, D.E., Longuet-Higgins, M.S., (1956) "The statistical distribution of the maxima of a random function," *In: Proceedings of the Royal Society of London. Series A, Mathematical and Physical Sciences,* Vol. 237, Issue 1209, pp. 212–232.

Campbell, K.W., (2003) "Prediction of Strong Ground Motion Using the Hybrid Empirical Method and Its Use in the Development of Ground-Motion (Attenuation) Relations in Eastern North America," *Bulletin of the Seismological Society of America,* Vol. 93, No. 3, pp. 1012-1033, June 2003.

Chandler, A. M., Lamb, N.T.K., Tsang, H.H., (2006) "Near-surface attenuation modelling based on rock shear-wave velocity profile," *Soil Dynamics and Earthquake Engineering,* 26, pp. 1004–1014.

Chandra, J., Guéguen, P., Bonilla, L.F., (2016) "PGA-PGV/Vs considered as a stress–strain proxy for predicting nonlinear soil response," *Soil Dynamics and Earthquake Engineering,* 85 (2016) 146–160.

Dawood, H. M., Rodriguez-Marek, A., Bayless, J., Goulet, C., Thompson, E., (2016) "A flatfile of ground motions from the KiKnet array," *Earthquake Spectra,* Vol. 32, pp 1281–1302, DOI:10.1193/071214EQS106.

Drouet, S., Cotton, F., Gueguen, P., (2010) "Vs30, κ, regional attenuation and Mw from accelerograms: Application to magnitude 3-5 French earthquakes," *Geophysical Journal International,* 182, 880–898.

Edwards, B., Faeh, D., D. Giardini, D., (2011) "Attenuation of seismic shear wave energy in Switzerland," *Geophysical Journal International,* 185, pp. 967–984.

Edwards, B., Ktenidou, O.-J., Cotton, F., Abrahamson, N., Van Houtte, C., Fäh, D., (2015) "Epistemic Uncertainty and Limitations of the κ0 Model for Near-Surface Attenuation at Hard Rock Sites," *Geophysical Journal International,* (2015) 202, 1627–1645.

Hashash, Y.M.A., Kim, B., Kottke, A.R., Rathje, E.M., Silva, W.J., Stewart, J.P., Campbell, K.W., (2014) "Reference-Rock Site Conditions for Central and Eastern North America: Part II – Attenuation (Kappa) Definition," *Pacific Earthquake Engineering Research Centre,* PEER 2014/12, August 2014.

Ji, C., Cabas, A., Bonilla, F., Gelis, C., (2020) "Quantifying the High-Frequency Spectra Decay Parameter Beyond the Linear-Elastic Regime," *under review,* 2020.

Konno, K. & Ohmachi, T., (1998) "Ground-motion characteristics estimated from spectral ratio between horizontal and vertical components of microtremor," *Bulletin of the Seismological Society of America,* 88 (1), 228–241.

Kottke, A. R., Rathje, E. M., (2008a) "Strata, Version alpha, Revision 381," *University of Texas,* Austin, TX.

Kottke, A. R., Rathje, E.M., (2008b) "Technical Manual for Strata, Report 2008/10," *Pacific Earthquake Engineering Research (PEER) Center,* University of California, Berkeley, CA.

Kramer, S., (1996) "Geotechnical Earthquake Engineering," Prentice Hall, Upper Saddle River, NJ.

Ktenidou, O.-J., Abrahamson, N.A., Darragh, R.B., Silva, W.J., (2016) "A Methodology for the Estimation of Kappa (κ) from Large Datasets: Example Application to Rock Sites in the NGA-

East Database and Implications on Design Motions," *Pacific Earthquake Engineering Research Centre,* PEER Report No. 2016/01, April 2016.

Ktenidou, O.-J., Cotton, F., Abrahamson, N.A., Anderson, J.G., (2014) "Taxonomy of κ: A Review of Definitions and Estimation Approaches Targeted to Applications," *Seismological Research Letters,* Vol. 85, No. 1, January/February 2014, doi: 10.1785/0220130027.

Ktenidou, O.-J., Gélis, C., Bonilla, L.-F., (2012) "A Study on the Variability of Kappa (κ) in a Borehole: Implications of the Computation Process," *Bulletin of the Seismological Society of America,* Vol. 103, No. 2a, doi: 10.1785/0120120093.

Ktenidou, O.-J., Van Houtte, C., (2012) "Empirical Estimation of kappa from Rock Velocity Profiles at the Swiss NPP Sites (19.02.2012)," Report TP2-TB-1090, *PEGASOS Refinement Project*.

Laurendeau, A., Cotton, F., Ktenidou, O.-J., Bonilla, L.-F., Hollender, F., (2013) "Rock and Stiff-Soil Site Amplification: Dependency on VS30 and Kappa (κ0)," *Bulletin of the Seismological Society of America,* Vol. 103, No. 6, December 2013, doi: 10.1785/0120130020.

Parolai, S., Bindi, D., (2004) "Influence of Soil Layer Properties on κ evaluation," *Bulletin of the Seismological Society of America*, 94:349–356.

Pilz, M., Cotton, F., Zaccarelli, R., Bindi, D., (2019) "Capturing Regional Variations of Hard-Rock Attenuation in Europe," *Bulletin of the Seismological Society of America,* Vol. 109, No. 4, pp 1401–1418, August 2019, DOI: 10.1785/0120190023.

Pilz, M., Fäh, D., (2017) "The Contribution of Scattering to Near–Surface Attenuation," *J Seismol,* (2017) 21:837-855, DOI 10.1007/s10950-017-9638-4.

Silva, W., Darragh, R., (1995) "Engineering characterization of earthquake strong ground motion recorded at rock sites," *Electric Power Research Institute,* Report TR-102261, Palo Alto, California.

Silva, W., Darragh, R., Gregor, N., Martin, G., Abrahamson, N., Kircher, C., (1998) "Reassessment of Site Coefficients and Near-Fault Factors for Building Code Provisions," Technical Report Program Element II: 98-HQGR-1010, Pacific Engineering and Analysis, El Cerrito, U.S.A.

Sonnemann, T., Halldorsson, B., (2018) "Towards an Automated Kappa Measurement Procedure," *In: Proceedings of the International Conference on Earthquake Engineering and Structural Dynamics*, Geotechnical, Geological and Earthquake Engineering 47, https://doi.org/10.1007/978-3-319-78187-7_4.

Thompson, E.M., Baise, L.G., Tanaka, Y., Kayen, R.E., (2012) "A Taxonomy of Site Response Complexity," *Soil Dynamics and Earthquake Engineering,* 41 (2012) 32–43.

Van Houtte, C., Drouet, S., Cotton, F., (2011) "Analysis of the origins of κ (kappa) to compute hard rock to rock adjustment factors for GMPEs," *Bulletin of the Seismological Society of America*, Vol. 101, pp. 2926–2941.

Bibliography

The following publications resulted from this project. One published paper, one under review and at least one more manuscript is currently being prepared for submission to a peer-reviewed journal. Additionally, results from this project are (or will be) presented at professional conferences (resulting in three peer-reviewed conference abstracts by the time this technical report was submitted):

Ji, C., Cabas, A., Cotton, F., Pilz, M., and Bindi, D. (2020), Within station variability in kappa: evidence of directionality effects. *Bull. Seism. Soc. Am* *https://doi.org/10.1785/0120190253*

Ji, C., Cabas, A., Bonilla, L.F., Gelis, C., (2020) Quantifying the High-frequency Spectral Decay Parameter Beyond the Linear-elastic Regime, Bull. Seism. Soc. Am. (under review)

Ji, C., Cabas, A., Al Atik, L., (2021) Near-surface attenuation estimates for low-to-moderate seismicity regions (in preparation)

Cabas, A., Ji, C., Bonilla, L.F., Gelis, C., (2021) Kappa and Material Damping: Insights from the Linear and Nonlinear Soil Behavior Regimes, 6th IASPEI / IAEE International Symposium: Effects of Surface Geology on Seismic Motion, Kyoto, Japan, March 15-17, 2021 (extended abstract)

Ji, C., Cabas, A., Bonilla, L.F., Gelis, C., (2020) Investigation of the correlation between kappa and soil nonlinearity, Oral presentation at the 2020 ES-SSA Annual Meeting [virtual conference] October 14-15, 2020.

Ji, C., Cabas, A., Bonilla, L.F., Gelis, C., (2020) Does Nonlinear Soil Behavior Affect Kappa Estimates? Poster presentation at the 2020 SSA Annual Meeting, Albuquerque, NM, April 27-30, 2020. [cancelled due to COVID-19] (abstract to be printed in Seismological Research Letters).